Earth Surface Processes and Landforms / Volume 44, Issue 1 / p. 160-178

Research Article | Full Access

How many measurements are required to construct an accurate sand budget in a large river? Insights from analyses of signal and noise

Paul E. Grams, Daniel Buscombe, David J. Topping, Matt Kaplinski, Joseph E. Hazel Jr

First published: 21 August 2018
https://doi-org.libproxy.nau.edu/10.1002/esp.4489
Citations: 12

FullText@NAU

Abstract

Morphological change in river channels is frequently evaluated in the context of mass balance sediment budgets. In a closed sediment budget, measurements of sediment influx and efflux are coupled with measured changes in channel topography to provide both spatial and temporal resolution, and independent estimates of the mass balance. For sediment budgets constructed over long river segments (~10^2 channel widths or greater) and long periods (~2 years or longer), spatial and temporal accumulation of measurement uncertainty, compounded by inadequate sampling frequency or spatial coverage, may produce indeterminate results. The degree of indeterminacy may be evaluated in the context of a signal-to-noise ratio (SNR), which is a function of the magnitude of the mass balance and the magnitudes of potential systematic uncertainties associated with measurements and incomplete sampling. We report on a closed sand budget consisting of measurements of flux and two morphological surveys for a 50-km segment of a large river over a 3-year period. Accurate reporting of the magnitude and sign of the change in sand storage was only possible by using state-of-the-art techniques with high temporal frequency and large spatial extent. Together, a sand flux and morphological mass balance revealed that sand evacuation was temporally concentrated (~100% of mass change occurred during 19% of the study period) and highly localized (70% of mass change occurred in 12% of the study segment). A SNR analysis revealed that uncertainty resulting from undersampling may approach or exceed that caused by measurement uncertainty and that daily sampling of suspended-sand concentration or repeat mapping of at least 50% of the river segment was required to determine the sand budget with SNR > 1. The approach used here to analyze sand budget uncertainty is especially applicable to other river systems with large temporal variability in sediment transport and large spatial variability in erosion and deposition. © 2018 John Wiley & Sons, Ltd.

Introduction

Sediment budgets quantify the sources, sinks, and transport pathways of sediment in contemporary and ancient systems (Hinderer, 2012) and are frequently applied to understand sedimentary system responses to land use and climate change (Owens *et al*., 2005; Hoffmann *et al*., 2010). In fluvial systems, the relation between sediment transport and morphological change is determined by constructing a sediment budget, also known as a sediment mass balance. Sediment budgets are typically computed using either a *flux-based*, or *morphological* method. A flux-based sediment budget comprises measurements of sediment influx, *I*, and efflux, *E*, which are summed over the sediment budget period and differenced to compute the mass balance, ΔS_f

$$I - E = \Delta S_f \tag{1}$$

In the flux-based sediment budget, *I*, *E,* and ΔS_f are typically computed in units of mass over the budget period. For a morphological budget, ΔS_m is computed in units of volume (L^3) as the difference between measurements of bed elevations made over the same river segment at the beginning of the budget period z_1 (L) and at the end of the budget period z_2 (L):

$$\Delta S_m = \sum a(z_2 - z_1) \tag{2}$$

where *a* is area (L^2) represented by each pair of repeat topographic measurements and the summation is over the river segment of interest. In a closed sediment budget, all flux terms of Equation 1 and all morphological terms of Equation 2 are measured or estimated and are related as

$$\Delta S_f = \Delta S_m(1 - \gamma)\rho \tag{3}$$

where γ is the bed porosity and ρ is the sediment density (ML^{-3}). It is widely recognized that uncertainty in measurements of flux (Topping *et al*., 2000b; Grams and Schmidt, 2005) or morphological change (Erwin *et al*., 2012; Schaffrath *et al*., 2015; Schimel *et al*., 2015) affect sediment budget computations and that those uncertainties may be large (i.e. of similar magnitude) relative to the computed mass balance (Erwin *et al*., 2012; Schaffrath *et al*., 2015; Warrick *et al*., 2015).

Measurements of any kind involve uncertainty, which typically includes both random errors and systematic errors. By definition, random errors are distributed across an entire dataset. In contrast, systematic errors are not necessarily spatially or temporally uniform and may affect all or part of a dataset. The relative magnitudes of random and systematic errors depend on the type of measurement, and the relative importance of each type of error

may vary depending on how the measurements are used. For example, elevation bias (a systematic error) could be inconsequential for morphological measurements that are used to examine feature morphology or for streamflow modeling. However, random errors could affect surface roughness estimates and cause bias in model predictions. Random errors also cause discrepancies between point elevations and DEM grid cell elevations (Lane *et al*., 2003). For sediment budgets that comprise many measurements over large spatial or temporal scales, random errors may be inconsequential because they cancel when spatially- or temporally-averaged. Small biases, however, can have a large impact on a sediment budget, because they are additive.

Systematic errors that cause uncertainty (potential bias) in sediment budgets were divided into two categories. The first category are those that are related to the measurements. These systematic errors may be caused by improper instrument calibration, a change in environmental conditions that affect measurements, or undetected operator mistakes. We refer to this category of potential bias as measurement uncertainty. The second category of systematic errors are those that are related to the sampling design, which we refer to as sampling uncertainty. Sampling uncertainty is distinct from measurement uncertainty, because these systematic errors are not related to instrument operation, but to the decisions of when, where, and how often to make measurements.

Decisions made in the sampling design may introduce sampling uncertainty into sediment budgets when measurements are not made at sufficient resolution to capture all relevant physical processes. For example, a mass balance computed from measurements of sediment flux may be affected by discharge-independent variations in sediment transport (Colby, 1964). This problem is common to many fluvial systems with weak or unstable sediment rating relations, often exhibited by hysteresis (Walling and Webb, 1988; Topping and Wright, 2016) that may result from changes in upstream sediment supply (Dinehart, 1998; Rubin *et al*., 1998; Topping *et al*., 2000a; Vericat and Batalla, 2006), lags between discharge and dune geometry (Julien *et al*., 2002; Kleinhans *et al*., 2007; Shimizu *et al*., 2009), or changes in the relative contributions of groundwater and surface runoff to streamflow (Andermann *et al*., 2012).

Sampling uncertainty may also affect sediment budgets computed from repeat morphological measurements, particularly for sediment budgets encompassing large areas where spatially comprehensive measurements are impractical or impossible. Owing to the difficulty of collecting accurate repeat morphological measurements in the channel and floodplain of large rivers, direct measurements of channel change have typically been limited to specific features (Ashworth *et al*., 2000), relatively short study reaches of ~10 to 20 channel widths (Lane *et al*., 2003; Grams *et al*., 2013), or discrete channel cross-sections (Pizzuto, 1994), which have been shown to introduce bias in calculations of morphological change (Lane *et al*., 1994). Many field studies show significant spatial variability in bank erosion and deposition (Hooke, 2007), and within-channel sedimentation (Grams *et al*., 2013). In these cases, insufficient morphological measurements, inadequate sampling of all depositional settings, or variations in bed-sediment composition or porosity may result in substantial bias in the estimate of sediment mass balance.

For some sediment budget applications, such as estimating long-term rates of landscape denudation or basin sediment yield (Nichols *et al*., 2005; Belmont *et al*., 2011; López-Tarazón *et al*., 2012), or to characterize short-term extreme events such as volcanic eruptions, landslides and dam breaks (Korup, 2012), the magnitude of sediment imbalance may outweigh uncertainties caused by measurement bias and sampling uncertainty. Climate and land-use changes are, however, driving a growing need for sediment budgets constructed over timescales of a few years to a few decades and over river segments comprising 100 s of channel units or more (McLean and Church, 1999; Slaymaker, 2003; Piegay and Hicks, 2005; Yang *et al*., 2007; Warrick *et al*., 2015). Depending on the specific system, a channel unit may be defined based on average channel width or depth, or the average spacing of a specific morphological unit such as dunes or bars. At scales of 100 s of channel units or more, which we refer to as *segment scale*, the sediment budget signal may be relatively weak compared with measurement and sampling uncertainties. In this situation, a signal that is small relative to temporal and/or spatial accumulation of measurement bias, and compounded by inadequate sampling frequency or spatial coverage, can result in indeterminate sediment budgets (Erwin *et al*., 2012). In these cases, it is especially important to consider potential bias contributed by both measurement- and sampling-related uncertainties.

The degree of indeterminacy (Kondolf and Matthews, 1991; Grams and Schmidt, 2005) in a sediment budget can be evaluated as a signal-to-noise ratio (SNR), in which the signal is the sediment balance, ΔS_f or ΔS_m, computed for a specified river segment and time interval (James *et al*., 2012). In this context we define noise as the spatially and/or temporally aggregated systematic measurement and sampling uncertainties that potentially overwhelm and obscure the budget signal. Use of this framework allows evaluation of the potential bias in a sediment budget in relation to systematic measurement errors, and potential bias introduced by the particular sampling frequency and/or spatial coverage. In this paper, we present an analysis of SNR that reveals how these aggregated uncertainties affect a segment-scale sand-only budget computation.

The sophistication and scope of modern mapping technologies (Lane *et al*., 2003; Tarolli, 2014; Passalacqua *et al*., 2015), in concert with recent developments in acoustical methods (Thorne and Meral, 2008; Topping and Wright, 2016) that enable monitoring suspended sand continuously (i.e. at 15-minute intervals) for multi-year periods, allow flux- and morphological-based sand budgeting at unprecedented scales and resolutions. The purposes of this paper are to (1) present a closed fluvial sand budget that is at the segment-scale (i.e. ~10^2 channel widths or greater) and computed from sub-daily measurements of sand flux and spatially extensive measurements of changes in bed morphology and sedimentology, (2) present an approach for evaluating both measurement- and sampling-related systematic uncertainty, and (3) illustrate the dual impact of measurement and sampling uncertainties on segment-scale sand budget estimates computed either from measurements of sand flux or measurements of morphological change. The closed sand budget is based on high-frequency measurements of sand flux and high-resolution morphological measurements of the submerged channel and exposed deposits from a portion of the Colorado River in Grand Canyon. The budget is also novel in that it utilizes repeat maps of bed-sediment composition at the same resolution and coverage as, and collected simultaneously with, the morphological measurements, through the application of an acoustical sediment classification method (Buscombe *et al*., 2014a, b). The results reveal both the power and the weaknesses of large-scale sediment budgeting and illustrate the sampling resolution required to detect the timing and spatial distribution of morphological change.

Study Area

Lower Marble Canyon (Figure 1) is a 50-km segment of the Colorado River within Grand Canyon National Park that begins 75 km downstream from Glen Canyon Dam and ends at the mouth of the Little Colorado River (Grams *et al*., 2013). Glen Canyon Dam, completed in March 1963, has eliminated snowmelt-driven floods in most years since dam closure (Topping *et al*., 2003) and in all years of the study period (Figure 2). Dam releases vary monthly and fluctuate hourly for hydroelectric power generation (Topping *et al*., 2003). Because the dam and reservoir block upstream sediment, the Paria River, which joins the Colorado River 25 km downstream from the dam, is the primary source of fine sediment (sand, silt, and clay) to Marble Canyon (Topping *et al*., 2000b). Although the river flows in a bedrock-walled canyon, the river bed is mostly sand and gravel (Buscombe *et al*., 2017), except where tributary debris fans consisting of boulders constrict flow and create rapids (Howard and Dolan, 1981). The debris fans also create downstream zones of lateral flow recirculation (Figure 3), known as *eddies* (Schmidt and Rubin, 1995), which are the most important morphological unit for sand storage (Hazel *et al*., 2006; Grams *et al*., 2013). Channel width at low discharge (~225 m^3/s) varies from less than 30 m at debris-fan caused constrictions to more than 150 m in expansions downstream from debris fans, with an average width of 100 m. There are 203 individual debris-fan created eddies within the study area that range in area from approximately 200 m^2 to 26,000 m^2. The average length of eddies is approximately 200 m, or twice the mean channel width. Thus, our *segment-scale* study area comprises approximately 500 channel widths, 203 eddy morphological units, and 250 eddy lengths. We refer to locations within the study area by river kilometer (Rkm), which is the distance downstream from Lees Ferry, Arizona along a digitized channel centerline. In this measurement system, the study area extends from Rkm 50 to Rkm 100 (Figure 1).

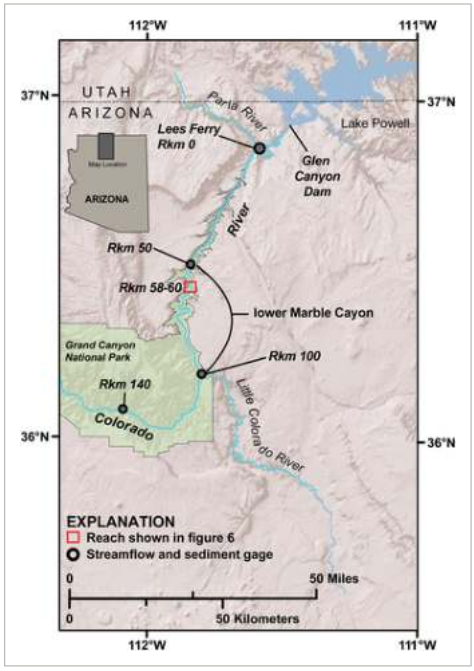

Figure 1

Open in figure viewer | PowerPoint

Map of Colorado River in the upstream portion of Grand Canyon National Park (outlined and shaded in green) showing lower Marble Canyon study segment and the location of stream gaging stations. Distances are in kilometers along the channel centerline (Rkm) downstream from Lees Ferry (Rkm 0). [Colour figure can be viewed at wileyonlinelibrary.com]

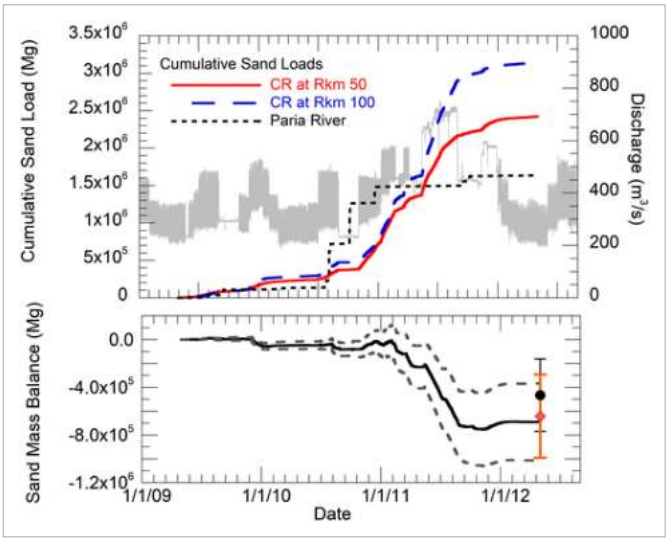

Figure 2

Open in figure viewer | PowerPoint

(Top panel) Instantaneous discharge for the Colorado River at Rkm 50 (light gray line). Cumulative suspended-sand loads between May 1, 2009 and May 1, 2012 for the Paria River at Lees Ferry (USGS station 09382000), Colorado River at Rkm 50 and Rkm 100. Except during periods of steady flow, discharge fluctuates daily and the line appears as a band that indicates daily maximum and minimum discharge. The high dam releases that occurred in 2011 are termed 'reservoir equalization flows' because they were released for the purpose of equalizing the reservoir storage volumes between Lake Powell and Lake Mead. (bottom panel) Lower Marble Canyon flux-based sand budget from the same period. Solid line shows accumulated mass balance based on difference between sand inputs at Rkm 50 (and estimated small tributary inputs) and sand export at Rkm 100 (Equation 1). Dashed lines define upper and lower bounds of uncertainty envelope (Equations 8 and 9). The morphological sand budget for the measured area is shown as round, black symbol for the same period (Equation 2), with uncertainty (Equation 13), and orange diamond showing the extrapolated morphological budget (Equation 19), with uncertainty (Equation 20). [Colour figure can be viewed at wileyonlinelibrary.com]

Figure 3

Open in figure viewer | PowerPoint

Illustration of debris-fan eddy complex showing depositional settings mapped at Rkm 66. The background image is an orthophotograph from aerial images collected in May 2009. For areas within the channel, the shaded relief image is a 25-cm resolution hillshade derived from the May 2012 multibeam sonar survey. For areas on the reattachment bar, separation bar, and debris fan, the shaded relief image is derived from a 1-m resolution digital elevation model based on May 2012 total station survey. [Colour figure can be viewed at wileyonlinelibrary.com]

One major goal of resource managers (US Department of the Interior, 2012) is to rebuild sandbars that have eroded since 1963 (Schmidt and Graf, 1990). Deposition of sand is at least temporarily accomplished by episodic release of controlled floods from Glen Canyon Dam that redistribute sand from the river bed to eddy sandbars (Hazel et al., 2010; Schmidt and Grams, 2011). Sandbars are of management interest because they form campsites used by river recreationists (Kearsley *et al*., 1994), support riparian ecosystems (Sankey *et al*., 2015), and are a source of windblown sand for upland cultural resources (Draut, 2012). Because sand supply is limited in the dam-regulated river (Topping *et al*., 2000b), controlled floods are scheduled based on the quantity of sand delivered by infrequent floods from the Paria River (Wright and Kennedy, 2011). Consequently, the flux-based sand budget is tracked to monitor sand supply so that the magnitude and duration of controlled floods may be scaled in proportion to the estimated sand supply (Grams *et al*., 2015). Repeat morphological measurements of sandbars and of the channel are used to evaluate changes in sandbars and in-channel sand storage, to describe the spatial distribution of those changes, and to provide an independent measurement of the sand storage. Future replication of these measurements will be used to evaluate the cumulative effects of a series of controlled floods on the sand budget.

Measurement and Computation of Flux-based Sand Budget

The flux terms of the sand budget, *I* and *E* in Equation 1, were computed from continuous (15-minute) measurements of streamflow and suspended-sand concentration (SSC) at stream gages on the Colorado River (Figure 1) and indirect measurements of sand input from ungaged small ephemeral tributaries. The budget computed in units of mass from flux measurements ΔS_f is

$$\Delta S_f = I_{susp} + I_{bed} + I_{trib} - E_{susp} - E_{bed} \tag{4}$$

where I_{susp} is the cumulative suspended-sand load measured at the stream gage at Rkm 50 (US Geological Survey station 09383050), I_{bed} is an estimate for cumulative bedload flux at Rkm 50, I_{trib} is the estimated sum of sand inputs from ungaged tributaries within the study segment, E_{susp} is the cumulative suspended-sand load measured at the stream gage at Rkm 100 (US Geological Survey station 09383100), and E_{bed} is an estimate for cumulative bedload at Rkm 100.

Streamflow at Rkm 50 and Rkm 100 was gaged using standard methods (Rantz, 1982) and SSC and grain size were measured with multi-frequency arrays of acoustical instruments (Griffiths *et al*., 2012; Topping and Wright, 2016) calibrated to conventional suspended-sand samples using the 2-frequency method described by Topping and Wright (2016). This method acoustically distinguishes between the sand and silt/clay fractions to determine the concentrations and grain sizes of each fraction independently. These data were used to compute 15-minute sand loads as the product of discharge and

SSC for each station for May 1, 2009 to May 1, 2012. Bedload transport was not measured continuously, but episodic measurements made by dune tracking indicate that bedload is ~5% of the suspended-sand load at Rkm 50 and Rkm 100 over a large range of flows (Rubin *et al*., 2001; Topping *et al*., 2010). Cumulative bedload influx was, therefore, computed as

$$I_{bed} = 0.05 I_{sand} \tag{5}$$

and the cumulative bedload efflux as

$$E_{bed} = 0.05 E_{sand} \tag{6}$$

There are no perennial tributaries within the study segment. Ephemeral tributaries are active only during short-duration seasonal rainfall events, which may also trigger debris flows and inputs of boulders, gravel, sand, and mud (silt and clay) (Webb *et al*., 1989). The silt and clay inputs are transported quickly downstream in the Colorado River mainstem as washload, causing increases in the silt-clay concentration at the Rkm 100 steam gage that are absent at the Rkm 50 stream gage (Topping *et al*., 2010). Based on episodic measurements of sand concentration in the tributary flows, we estimate I_{trib} was 14% ± 50% of the measured increase in the cumulative silt and clay loads between the Rkm 50 I_{mud} and Rkm 100 E_{mud} gages,

$$I_{trib} = 0.14(E_{mud} - I_{mud}) \tag{7}$$

Uncertainty in the cumulative sand loads over longer timescales (i.e. >multiple days) results from small, undetected, possibly persistent biases in discharge measurements (Sauer and Meyer, 1992), stage–discharge relations (Kiang *et al*., 2016), physical suspended-sand samples (Topping *et al*., 2010; Sabol and Topping, 2013), or acoustical suspended-sand measurements (Topping and Wright, 2016). Because the cumulative sand loads computed over periods of months to years are based on a very large number of individual measurements of SSC made at 15-minute intervals, we assume that random measurement errors (described in detail in Topping and Wright, 2016) cancel to zero over the 3-year period of this study. Some systematic errors may, however, persist undetected, causing potential bias in the sand budget. This is evidenced by Topping *et al*. (2010) who analyzed repeat measurements of SSC made at closely spaced cross-sections, and estimated that persistent biases may result in a maximum probable deviation from computed sand budgets of up to ± 5% over months to years in our study area. Here (and in the morphological sand budget, below), we estimate uncertainty as the *maximum probable bias*, which we define as the maximum likely systematic error that may be temporally or spatially persistent and potentially affect the computed sand budget. Because this is a bias and not a random error, we do not assume a normal distribution and cannot assign a specific confidence level, but consider our estimates to be approximately comparable with a 95% confidence level.

The uncertainties in mainstem flux and tributary inputs are incorporated in the budget, conservatively computing the worst case combinations of the signs of the individual uncertainties. The lower bound of the sand budget was therefore calculated as

$$\Delta S_{LB} = (I_{sand} + I_{bed})(1 - U_f) + I_{trib}(1 - U_{trib}) - (E_{sand} + E_{bed})(1 + U_f) \tag{8}$$

where uncertainty in the mainstem sand loads U_f = 0.05 and uncertainty in the tributary inputs U_{trib} = 0.5. The upper bound of the sand budget is,

$$\Delta S_{UB} = (I_{sand} + I_{bed})(1 + U_f) + I_{trib}(1 + U_{trib}) - (E_{sand} + E_{bed})(1 - U_f) \tag{9}$$

The instantaneous values for discharge, SSC, and sand budgets determined by this method for any time interval beginning in 2002 may be computed interactively online at www.gcmrc.gov/discharge_qw_sediment (Sibley *et al*., 2015).

Analysis of signal and noise in the flux-based sand budget

The high temporal resolution flux data were systematically subsampled, and the sediment budget recomputed upon each subsampling, to simulate the uncertainty that would be contributed by sample frequency and measurement uncertainty with progressively lower sample frequency. Recall that we define measurement uncertainty as the potential bias that, in this case, could be caused by improper instrument calibration, or the result of environmental conditions outside the calibration. This simulation was achieved by resampling the 15-minute record of SSC and discharge at increasing sample intervals and, at each new sample interval, recomputing ΔS_f as a function of increasing interval up to a maximum interval of 104 days. The measurement interval was increased in 15-minute increments for sample intervals between 15 minutes and 24 hours (which is exactly the period of the discharge wave due to regular releases from Glen Canyon Dam). Thereafter, the sample interval was increased in 24-hour increments up to the maximum interval of 104 days. For each sample interval, new time-series of SSC and discharge were created by sampling measurements at the desired interval from among all the samples in the time-series at each gage. For measurement intervals between 15 minutes and 24 hours, all possible sample sets were evaluated (i.e. there is only one possible measurement set for a 15-minute sample interval, two possible sets for a 30-minute interval, etc.). For measurement intervals between 2 days and 104 days, 100 measurement sets at the desired interval were drawn randomly. The suspended-sand flux at each gage was recomputed for each of the 1 to (up to) 100 realizations of simulated time-series, per sample interval, by integrating sand concentration and discharge between simulated sample times (Porterfield, 1972; Horowitz *et al*., 2015), and recomputing the cumulative loads at the two gages. This subsampling approach to recomputing cumulative loads is similar to that described by Thomas (1985) and Thomas and Lewis (1995). The alternative approach of recomputing fluxes using a rating curve between the logarithms of discharge and sand concentration (Cohn, 1995; Horowitz *et al*., 2015) was considered but ultimately not adopted because of the well-documented biases this approach introduces (Ferguson, 1986; Cohn, 1995), and because of a lack of statistical power at very large sample intervals of weeks to months.

SNR is a relative measure, often therefore expressed in decibels, of the signal power to the noise power. The boundary between low and high SNR is usually considered to be 2 (3 dB). Often, the signal is not considered stochastic, but the noise always is (Cover and Thomas, 1991; Smith, 2003). An accepted definition of SNR from signed random measurements is the ratio of the mean to the standard deviation (Schroeder, 1999; Smith, 2003). Therefore, SNR in the flux-based budget associated with subsampling noise, SNR_{fs}, was computed as

$$SNR_{fs} = \frac{\Delta S_f}{\sigma_{\Delta S_s}} \tag{10}$$

where ΔS_f is the sand mass balance based on the 15-minute record, and was therefore constant, and the noise was computed per sample interval as the standard deviation of each set of 100 computed sand mass balance estimates from the resampled time-series, $\sigma_{\Delta S_s}$. The measurement uncertainty noise was similarly computed from the standard deviation of recomputed fluxes factoring in the measurement uncertainty bounds. With reference to Equations 8 and 9, given the symmetry with which the upper and lower bounds bracket the computed mass balance, SNR associated with measurement noise, SNR_{fm}, need only be computed using one uncertainty bound, such as

$$SNR_{fm} = \frac{\Delta S_{fUB}}{\sigma_{\Delta S_{mp}}} \tag{11}$$

Our estimate of measurement uncertainty (5%) is based on analysis of the 15-minute record of suspended-sand concentrations, discharge, and cumulative loads computed from those measurements. The estimate may, therefore, include an unknown proportion of uncertainty associated with that sample frequency in addition to uncertainty associated strictly with the measurements of suspended sand. Indeed, complete isolation of the causes of potential bias may be intractable. Thus, the noise in the flux budget that we attribute to subsampling may be described as the added uncertainty associated with measurement intervals greater than 15 minutes. The noise caused by subsampling and the noise caused by measurement uncertainty are not independent (both could result from unmeasured or unknown variability in discharge or SSC) and are therefore summed by simple addition to estimate total noise and SNR_{fT}, the SNR associated with subsampling and measurement uncertainty considered together.

Measurement and Computation of Morphological Sand Budget

Computation of the morphological sand budget for the 50-km segment of the Colorado River required the development of methods to utilize measurements from multiple platforms (topographic measurements for sand deposits above water and bathymetric measurements for deposits below water), segregate measurements among depositional settings, account for areas where, during either of the two surveys, mapping was not feasible or where the bed surface comprised sediment coarser than sand, and to estimate uncertainty. In the following sections, we describe the process used to compute two versions of the sand budget: (1) as the sum of measured bed elevation changes (Equation 2), with no extrapolation to unmapped areas; and (2) as the sum of measured bed elevation changes with extrapolation to areas where topography and bathymetry were not measured. Both estimates account for measurement uncertainty and uncertainty in bed-sediment composition and neither estimate uses a minimum level of detection threshold (Brasington *et al*., 2000). The estimate with extrapolation includes an estimate of uncertainty for extrapolated changes in the unmeasured areas that is based on the SNR analysis.

Measurement of topography, bathymetry, and bed composition

Channel and bank morphology (i.e. undifferentiated topography and bathymetry) were measured on river expeditions that occurred May 3 to May 16, 2009 and May 5 to May 16, 2012. The goal of the mapping campaigns was to measure as much of the active sand (the distinction between active and inactive sand is described below) as feasible within navigability and trip-length constraints (the study area is accessible only by multi-day river expedition). Bathymetry was measured using a multibeam sonar (Reson 8125 in 2009 and Reson 7125 in 2012) and Odom CV-100 singlebeam sonar, and topography was measured with an optical total station (i.e. theodolite with electronic distance meter). Multibeam sonar was the primary bathymetric mapping method and was used where water depth was greater than ~2 m. The only significant difference between the two multibeam sonar systems used, for the purposes of the present study, manifested in the spatial density of soundings, which was marginally higher in 2012. Singlebeam sonar was used for water depths between ~ 2 m and ~ 0.5 m. Total stations were used for exposed deposits and water depths less than ~ 0.5 m. The methods for data collection and data processing to produce a digital elevation model (DEM) on a regular grid with 1-m resolution (grid node spacing) were described by Grams *et al*. (2013), Hazel et al. (2008), and Kaplinski *et al*. (2017b). Measurements were made throughout the entire study segment comprising 50% of the total area of the alluvial valley bottom (active and inactive deposits) and 71% of the area defined as active channel and active fine-grained deposits (Table 1). Approximately 72% of the region represented in the final DEM was measured with multibeam sonar in both years and 6% was measured by total station survey in both years. The remaining 22% was measured by singlebeam sonar in both years, or by a different method in each year.

Table 1. Depositional settings in study area and proportion of each setting that was mapped and included in digital elevation model

Active channel and fine-grained deposits				
Channel within eddy	897 585	15%	603 894	67%
Channel adjacent eddy	1 526 958	26%	1 144 702	75%
Pools in channel	1 234 874	21%	911 863	74%
Sandbars in eddies	220 438	4%	122 864	56%
Sandbars along channel margins	27 070	0.5%	2 985	11%
Subtotal - Active	3 906 925	66%	2 786 308	71%
Inactive channel and coarse-grained deposits				
Channel in rapids and riffles	1 161 702	20%	180 827	16%

Sandbars in eddies above CF stage	442 270	7%	10 425	2%
Sandbars along channel margins above CF stage	187 502	3%	1,393	1%
Gravel bars	213 033	4%	4	0%
Subtotal - Inactive	2 004 506	34%	192 649	10%

Because the river bed in the study area varies among sand, gravel, cobble, boulder, and bedrock, it was necessary to consider bed-sediment composition when constructing the sand budget. We classified bed sediment for all regions measured by multibeam sonar based on acoustic backscatter using the methods detailed by Buscombe *et al*. (2014a, b). We used a 3-class form of this method to classify the bed, also at 1-m resolution, into regions of (1) *sand*, (2) *gravel*, and (3) *rock* (undifferentiated cobble, boulder and bedrock). Silt and clay deposits are exceptionally rare, as is submerged aquatic vegetation. This fully-automated classification was calibrated and verified based on observations of the bed made by underwater video camera (Rubin *et al*., 2007; Buscombe, 2013). Because automated classification was possible only where data were collected with multibeam sonar, it was necessary to estimate bed composition for the regions mapped by singlebeam sonar and by total station. All regions within eddies that were not classified as either rock or gravel were classified as *likely sand*. We also included in this category regions of the channel bed that were mapped by singlebeam sonar in either the 2009 or the 2012 survey and mapped by multibeam sonar in the other survey and classified as sand. This assumption is reasonable, because we focused field data-collection efforts on regions with sand substrates. The bed composition was classified as *no data* for regions in the channel that were not mapped by multibeam sonar in either year. The DEMs and bed composition classifications are available in Kaplinski *et al*. (2017a; 2018).

Map of depositional settings for budget segregation

Depositional settings were digitized on-screen in a geographic information system with reference to a basemap consisting of high-resolution (20 × 20 cm) aerial photo images (Davis, 2012) collected in May 2009 during a period of approximately steady dam releases (227 m^3/s). The map includes exposed deposits and depositional settings below the water surface at the time the images were collected, because the largest changes in sand volume occur within the wetted channel below the stage associated with the discharge of 227 m^3/s (Hazel et al., 2010). Deposits within eddies (Figure 3) were mapped based on morphology according to the terminology of Schmidt and Graf (1990) and Schmidt *et al*. (1999); and include separation bars (which occur near the flow separation point), reattachment bars (which project upstream from the flow reattachment point), upper-pool bars (which occur in the eddy upstream from the debris fan), and undifferentiated eddy bars (which typically occur by fusion of separation and reattachment bars). Eddies were mapped by identifying the upstream point of flow separation, the downstream point of flow reattachment, and connecting those points with the average line dividing downstream-directed flow from recirculating flow in the eddy. These features are identifiable in the aerial images, because the different characteristics of the water surface in eddies and the main channel typically cause differences in light reflectivity. The division between eddy and main channel approximately follows the break in slope between the submerged portion of the eddy sandbar and the main channel (Figure 3). Eddies typically lengthen as streamflow increases (Rubin *et al*., 1990; Schmidt, 1990), so the line dividing the eddy from the main channel extends to the downstream end of the sandbar in the reattachment zone (Figure 3). The wetted channel was further subdivided into (1) channel adjacent to eddies, (2) channel in rapids or riffles adjacent to debris fans, (3) channel in rapids or riffles not adjacent to debris fans, and (4) channel in all other locations. The preliminary map was inspected in the field and edited to produce the final map.

The depositional settings described above were grouped into active and inactive deposits. Active deposits comprise all sand in the channel and bare sand deposits on the banks. The channel within rapids and riffles, exposed gravel bars, and sand deposits that are covered with dense vegetation with surfaces above the elevation inundated by controlled floods were classified as inactive deposits. The active deposits are considered most likely to exhibit measureable change in bed elevation within the regime of dam releases, including controlled floods. Only by focusing the topographic and bathymetric measurements on the active deposits, was it feasible to map a large fraction of the study segment (Table 1).

Computation of morphological sand budget

The morphological sand budget (Equation 2) was computed from the cell-by-cell differences in elevation between the co-registered 1-m resolution DEMs developed from the May 2009 and May 2012 topographic/bathymetric surveys. The resulting DEM of difference (DoD) was analyzed to compute erosion, deposition, net volume change, and uncertainty aggregated by depositional setting and 100-m river segment. Comparisons between the morphological budget and the flux-based budget were made using Equation 3 with particle density, ρ, of 2650 kg/m^3 and porosity, γ, of 40% (Curry *et al*., 2004).

Uncertainty in the morphological sand budget computed in units of volume may be caused by (a) measurement bias, δ_m, (b) uncertainty in the composition and properties of eroded or deposited material (i.e. sand or otherwise, porosity, density), δ_c, and (c) unknown changes in those parts of the study area where topographic measurements were not made (i.e. sampling uncertainty, δ_s). For computation of net change in bed volume over areas of the bed comprising many measurements (i.e. 100 s to 1000s of grid cells), normally-distributed random errors cancel to zero and δ_m results entirely from potential bias. Such systematic errors may result from undetectable survey errors, improper equipment calibration, or changes in environmental conditions that affect optical instruments (temperature, pressure, etc.).

We quantified the potential bias in mean elevation change for each measurement method. For regions mapped with multibeam sonar, this was achieved by evaluation of fiducial regions (cf. Brock *et al*., 2001), which are stable features such as individual large flat boulders, regions of bedrock, and regions of the bed covered by immobile cobbles. This approach provides an estimate of the maximum probable bias in sand volume computed as $U_{mb}A$, where U_{mb} is the maximum estimated systematic error in elevation change for regions mapped by multibeam sonar and A is the area of the region over which mean

elevation is computed. Although the DEMs are 1-m resolution, we compute ΔS_m (Equation 2) at the scale of the mapped depositional settings (e.g. eddies) or aggregations of those features at the scale of 100-m river segments. The depositional settings vary in size, but typically comprise regions of the bed greater than 100 m^2. The 79 individual fiducial regions we analyzed are distributed throughout the study area and range in area from 1 m^2 to over 6000 m^2, which is of the same order as the depositional settings and 100-m segments. Thus, this approach provides a quantification of uncertainty at the same spatial scale over which bed elevation change is computed for the sand budget. For each fiducial region, we computed the mean difference in elevation between the two surveys. The absolute error was less than 0.08 m for every polygon, the mean signed error among all 79 polygons was –0.01 m with standard deviation, σ = 0.03 m, and the mean absolute error was 0.02 m (Figure S1). Based on this analysis, we use 0.06 m (2σ) for U_{mb} (where the 95% confidence error is 1.96σ for a Gaussian normal distribution). We emphasize that this is not an estimate of random error, but an estimate of maximum probable systematic error that is analogous to the maximum probable persistent bias used in the flux-based sand budget. The same value is used for U_{mb} when ΔS_m is computed over a single geomorphic unit as is used for the budget computed over the entire study area, because the potential sources of systematic error cannot be assumed to be independent (therefore, they are additive) and because analysis of uncertainty as a function of fiducial region size indicates that σ does not decrease below 0.03 m (Figure S2).

The maximum probable systematic uncertainty in elevation change for regions measured by conventional total station, U_{ts}, was estimated as 0.04 m, based on error analysis by Hazel et al. (2010); and the maximum probable systematic uncertainty in elevation change for regions mapped using singlebeam sonar, U_{sb}, was estimated as 0.12 m, based on error analysis by Kaplinski *et al*. (2014). These estimates of uncertainty were multiplied by the area of each respective measurement method to compute total measurement uncertainty, using

$$\delta_m = U_{mb}A_{mb} + U_{ts}A_{topo} + U_{sb}A_{sb} \tag{12}$$

where A_{mb} is the area mapped by multibeam sonar, A_{topo} is the area mapped by topographic survey, and A_{sb} is the area mapped by singlebeam sonar. For areas mapped using different methods in each year, the area that was included was that with the greatest uncertainty.
We used the bed-sediment classification and the map of depositional settings to estimate uncertainty in the composition of the computed morphological changes. We have high confidence that the volume represented by morphological change in a given grid cell was entirely sand where the bed surface was classified as sand in either or both surveys, and also those grid cells within eddies, even if the bed was not explicitly classified, because extensive previous work has established that the bed surfaces in eddies consist mostly of sand. Where the bed was never classified as sand (rock or gravel in both years or classified as rock or gravel one year and unclassified the other year), we have weak confidence that the volume of material representing the morphological change in a particular grid cell was composed entirely of sand and classify that volume as possibly sand. We use that computed sediment volume change for those areas of the bed where the change possibly comprised sand as the estimate of maximum probable uncertainty based on bed composition, δ_c. Note that this volume was included in the budget estimate, because sand often fills the interstices of, and may even bury, gravel and rock. Therefore erosion or deposition in those regions could consist entirely of sand even if classified otherwise and δ_c represents an upper bound on sand volumes thus unaccounted for.

For the morphological sand budget without extrapolation, measurement bias and volumetric uncertainty associated with ambiguity in composition are treated as independent systematic errors and summed in quadrature (Taylor, 1997) to compute total uncertainty in the morphological budget δ_T,

$$\delta_T = \sqrt{\delta_m^2 + \delta_c^2} \tag{13}$$

Analysis of signal and noise in the morphological sand budget

Although the morphological measurements were of high resolution and spatially extensive, they still comprised just 71% of the active deposits in the study area (Table 1). The SNR analysis of the morphological measurements was used to (1) examine the effect of changing spatial coverage on the computed morphological budget, and (2) provide an estimate of the uncertainty associated with extrapolating the morphological budget to include the portion of the study area where measurements were not made. This was achieved by systematically subsampling the morphological measurements, and recomputing the sediment budget upon each subsampling, to simulate the uncertainty associated with decreasing sample coverage.

The morphological changes were subsampled by dividing the DOD for the study area into 408 segments, each 100 m in length in the streamwise direction. We incrementally decreased the number of samples from 408 to 1, resulting in samples that comprised 100% to 0.2% of the measurement area. For each sample size, the area-weighted average elevation change over the area sampled $\overline{\Delta z}_s$ was computed as

$$\overline{\Delta z}_s = \frac{\sum \Delta V_i}{A_s} \tag{14}$$

where ΔV_i is the volume change in each of the included segments, the summation is over all included segments, and A_s is the total area of all segments included in the sample. The estimated budget for the sample was then computed as

$$\Delta S_{ms} = A_m \overline{\Delta z}_s \tag{15}$$

where A_m is the constant total area of the original set of morphological measurements. This process was repeated 100 times, resulting in a distribution of ΔS_{ms} values for each sample size from which the mean $\overline{\Delta S}_{ms}$ and $\sigma_{\Delta ms}$ among those iterations was calculated. The method for computing SNR for sampling uncertainty from the morphological measurements, SNR_{ms}, was analogous to the method used to compute SNR_{fs} in the flux-based budget and was computed as the ratio between the sand budget computed from the entire set of measurements (constant) and the standard deviation among the iterations,

$$SNR_{ms} = \frac{\Delta S_m}{\sigma_{\Delta ms}} \tag{16}$$

The measurement uncertainty SNR_{mm} was computed as the ratio between the measured budget and the sum of the uncertainty in all segments, $\sum \delta_m$, regardless of the number of segments sampled and was, therefore, constant (i.e. measurement uncertainty was included both for the sampled and unsampled segments for each sample size).

$$SNR_{mm} = \frac{\Delta S_m}{\sum \delta_m} \tag{17}$$

Finally, SNR_{mT}, including both sampling and measurement uncertainty was computed as

$$SNR_{mT} = \frac{\Delta S_m}{(\sigma_{\Delta ms} + \sum \delta_m)} \tag{18}$$

Note that our estimates of measurement uncertainty in both the morphological and flux-based sand budgets are estimates of the maximum probable systematic uncertainty (bias) for spatially and temporally aggregated budgets, respectively. We use this approach, because systematic errors, by definition do not have an expected value and use of the most probable range, which is ultimately based on some degree of judgment, is most appropriate. The sampling uncertainty, however, can only be addressed by stochastic simulation, in which case the standard deviation of the resulting distribution is the most appropriate measure of variability. These differences should be considered when the two components of uncertainty are combined or compared.

Extrapolation of the morphological sand budget

We computed an extrapolated morphological sand budget, ΔS_{mEx}, by estimating changes in sand volume for locations where measurements were not made as the product of the area-weighted mean change in sand elevation where measurements were made, $\overline{z}_{ad}$, and the total area of active deposits in the map of depositional settings where measurements were not made and adding those changes to ΔS_m:

$$\Delta S_{mEx} = \Delta S_m + \overline{z}_m[A_T - A_m] \tag{19}$$

where A_T is the total area of active deposits. We estimate uncertainty in the extrapolated portion of the sand budget as the standard deviation, $\sigma_{\Delta ms}$, from the SNR analysis computed for the percentage of the measured morphological changes that is equivalent to the percentage of the entire study area where morphological measurements were collected (Table 1),

$$\delta_s = \sigma_{\Delta ms(71)} \tag{20}$$

where the subscript (71) refers to the percentage of the reach mapped. This extrapolation of the budget to unmeasured areas and the associated estimate of uncertainty necessarily assume that the distribution of morphological changes in the areas that were not measured is similar to the distribution in the areas measured. The SNR analysis, which shows the percentage of the reach that must be mapped to achieve SNR > 2 provides justification for this assumption.

Results

Sand budget for lower Marble Canyon

The flux-based and morphological sand mass balances were both negative, indicating net erosion from lower Marble Canyon between May 2009, and May 2012 (Figure 2). During this period, 2.54 ± 0.13 × 10^6 Mg of sand entered lower Marble Canyon at Rkm 50 and 3.29 ± 0.16 × 10^6 Mg of sand exited lower Marble Canyon past Rkm 100 (Figure 2). Ungaged tributaries added an estimated 51 000 ± 25 500 Mg of sand to the reach, resulting in a flux-based sand budget of –702 000 ± 317 000 Mg (–442 000 ± 200 000 m^3). The repeat morphological surveys show 761 100 m^3 of erosion and 465 400 m^3 of deposition resulting in a measured net change of –293 500 ± 190 770 m^3 (–466 700 ± 303 300 Mg) for the same period (Table 2). The flux-based and morphological estimates of net erosion differed by about 150 000 m^3 (equivalent to about 0.03 m of sand distributed evenly throughout the study area). Although the difference between the flux-based and morphological budgets is large, the two budgets agree within the uncertainty bounds.

Table 2. Morphological sand budget

Onshore sandbars	125 800	na	100%	21 300	-48 700	-27 300	6,300		6,300
Eddies	603 900	64%	83%	251 100	-240 900	10 200	45 300	7,700	45 950
Channel adjacent eddy	1 144 700	91%	74%	122 600	-351 600	-229 000	56 900	42 500	71 020
Other Channel	1 092 700	80%	88%	70 400	-120 000	-47 400	74 200	4,600	74 342
Total	2 967 100	77%	86%	465 400	-761 100	-293 500	182 700	54,900	190 770

Together, the flux and morphological measurements reveal both temporal and spatial distributions of change in sand storage. The flux measurements show that sand storage was stable for 2009 and 2010 and that all of the net erosion occurred between March and September 2011 (Figure 2). This period of erosion coincided precisely with a period of sustained high releases from Glen Canyon Dam that transferred water from Lake Powell to Lake Mead, as required by interstate water allocation agreements (US Department of the Interior, 2007). The repeat morphological measurements show that both erosion and deposition occurred throughout lower Marble Canyon in all depositional settings (Figure 4). The net change in sand thickness averaged over the mapped area in lower Marble Canyon was approximately –0.08 m (Table 2), but spatially variable within and among the depositional settings. Changes in mean deposit elevation within each mapped deposit, for example, were typically less than 1 m, but ranged from approximately –2 m to 2 m (Figure 4). Deposition and erosion were consistently largest in eddies (Figure 4); however, the magnitudes of each were approximately balanced and net change in sand storage within eddies was therefore very small. The large majority of net changes in sand storage occurred in segments of the channel adjacent to eddies (Table 2), where erosion was consistently larger than deposition (Figure 4). These segments of channel include scour holes that typically occur downstream from rapids or riffles and pool exit slopes where the bed rises from the downstream end of the scour hole (Figure 3). Both the magnitude and the spatial variability of morphological change were much less in other channel settings than in eddies or in the channel adjacent to eddies (Figure 4).

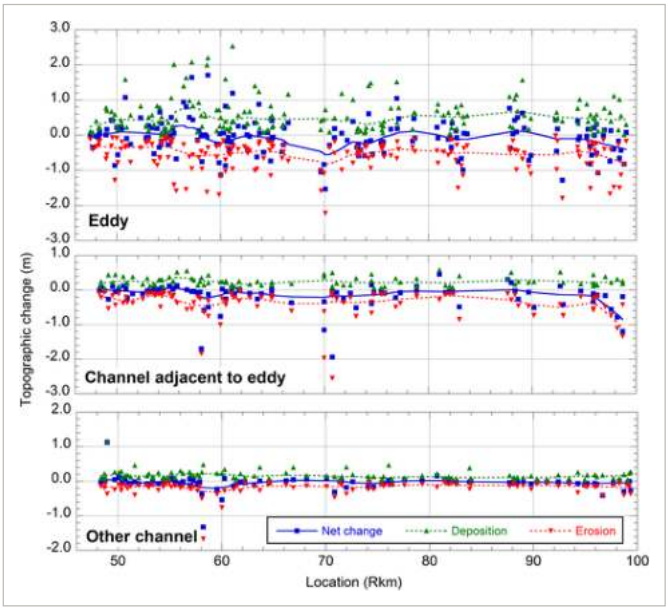

Figure 4

Open in figure viewer | PowerPoint

Average change in sand thickness for eddy, channel adjacent eddy, and other channel depositional settings (blue squares). The mean thickness of deposition (volume of deposition divided by area of deposition) and the mean thickness of erosion (volume of erosion divided by area of erosion) are shown by the upward and downward pointed green and red triangles, respectively. The lines show moving averages, weighted over approximately 5-km intervals. [Colour figure can be viewed at wileyonlinelibrary.com]

Most of the net erosion from the channel adjacent to eddies occurred in just three short reaches (Figure 5). Approximately 32 000 m^3 of sand was eroded from the reach between Rkm 58 and 60 (Figure 6), 58 000 m^3 was eroded between Rkm 70 and 71, and 113 000 m^3 was eroded between Rkm 96 and 99. Together, evacuation of sand from these segments, which comprise 12% of lower Marble Canyon, accounted for about 70% of the measured net volume loss.

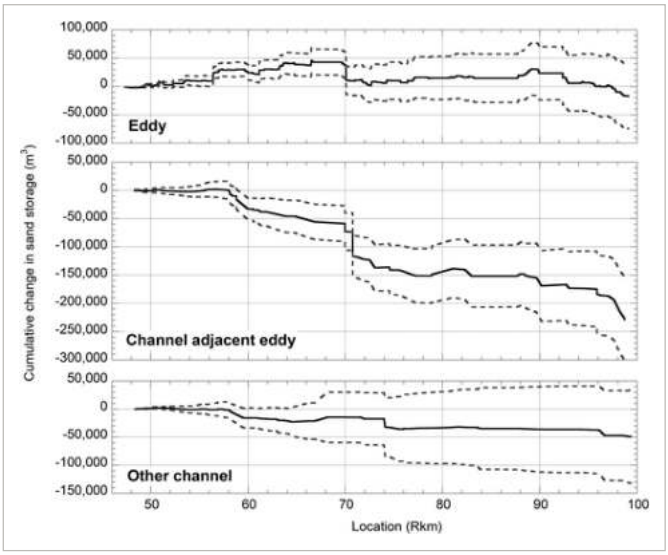

Figure 5

Accumulated change in sand storage from Rkm 50 to Rkm 100. Center black line is the accumulated net volume difference between the May 2009 and May 2012 DEMs. The gray dashed lines define the range of measurement uncertainty δ_m for the morphological budget (Equation 12).

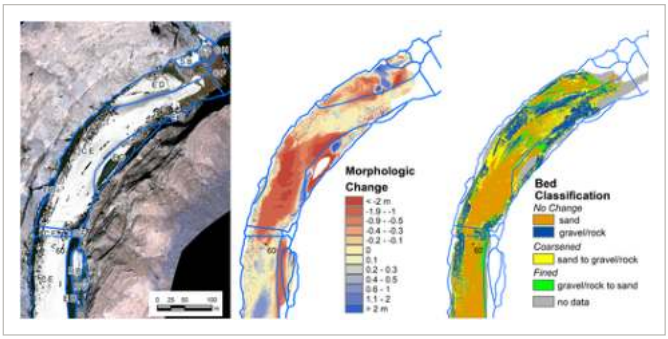

Figure 6

Map of segment beginning at Rkm 58 showing from left to right: shaded relief map created from the May 2012 DEM with orthophotograph background, morphologic change between May 2009 and May 2012, and change in bed composition for the same period. The depositional settings are shown in blue and labeled in the left panel, using the codes listed in Figure 3. Streamflow is from upper right to lower left and all maps are at the same scale.

The parts of sandbars where sand is exposed above the water surface at low discharge, and which are used recreationally as campsites, are of the greatest management interest. Those regions, however, compose a relatively small proportion of the total channel area and sand budget. Approximately 5% of the volume of deposition, 8% of the volume of erosion, and 11% of the net change in sand storage in Lower Marble Canyon was derived from the subaerial regions of sandbars for this period (Table 2). Although the volumes of erosion and deposition from subaerial sandbars were each small relative to the volumes of change in the rest of the eddy, there was a greater proportion of erosion from the subaerial sandbars than from elsewhere in eddies, where net deposition occurred (Table 2). Thus, eddies as a whole retained sand during this period of sand evacuation and the exposed sandbars in eddies experienced net erosion.

During the 2009 to 2011 period of net erosion of sand from lower Marble Canyon, the proportion of the bed surface covered by sand decreased in the channel and was stable in the eddies. Overall, up to 90% of the bed in eddies and approximately 50 to 70% of the bed in the channel was sand in the regions mapped (Figure 7). In eddies, the area of sand increased slightly while the area of gravel and rocks decreased almost concomitantly (Figure 7 and Table 3). In the channel, however, the area of sand decreased and the area of gravel increased.

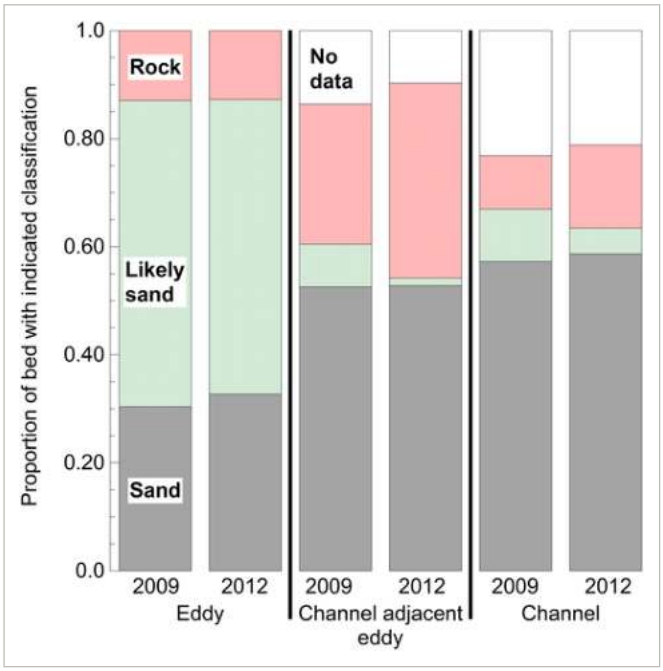

Figure 7

Estimated bed surface composition for 2009 and 2012 in eddies, channel adjacent eddies, and other channel locations for all areas of lower Marble Canyon included in topographic comparison between 2009 and 2012.

Table 3. Bed-sediment classification transition probability matrices. Cells shaded gray indicate those transitions where morphologic change was considered sand

		No data	Not sand	Sand
2009	No data	0.83	0.04	0.13
	Not sand	0.11	0.42	0.47
	Sand	0.21	0.16	0.63
	Channel		2012	
		No data	Not sand	Sand
2009	No data	0.54	0.13	0.32
	Not sand	0.04	0.70	0.26
	Sand	0.06	0.18	0.77

Although sand decreased in area slightly (1–3%, depending on depositional setting) as sand was eroded from the channel, the locations of most sand patches did not change between 2009 and 2012. Most of the erosion occurred from regions classified as sand in 2009 that remained sand in 2012. The proportion of the bed with measured variability in sand coverage (transition from sand to not sand or vice versa) ranges from zero up to about 20% of the bed surface, and these regions typically occurred around the edges of the sand patches (Figure 6). The large degree of persistence of most sand patches despite substantial decreases in surface elevation suggests that they are hydraulically forced, not freely migrating, and also suggests the existence of reservoirs of sand in the bed in those locations that are thicker than the observed changes in bed elevation.

Signal and noise in the sand budget

The standard deviation of computed mass balances increases exponentially with increasing sample interval, and therefore the inverse trend is observed in the SNR_{fs} (Figure 8). The noise contributed by measurement uncertainty and the noise contributed by subsampling are of similar magnitude and individually cause the sand budget to become indeterminate (that is, SNR falls below 1) for sample intervals of 7 (measurement noise only) to 10 (subsampling noise only) days. Accounting for both sources of noise (i.e. the solid line in Figure 8), the flux-based sand budget becomes indeterminate for sample intervals greater than 2 days. Sub-daily sampling would be required for $SNR_{fT} \geq 2$.

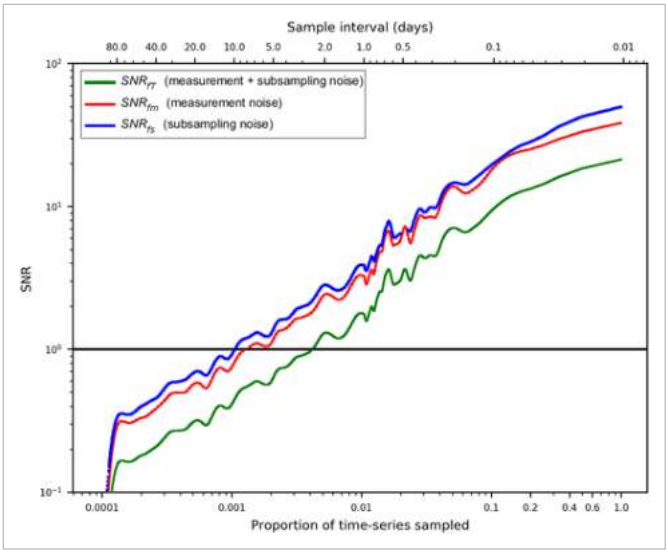

Figure 8

Open in figure viewer | PowerPoint

The signal-to-noise ratio (SNR) for flux-based method as a function of SSC sample interval (top axis). Sample interval is also shown as the proportion of the complete 15-minute interval time-series sampled (bottom axis). Noise contributed by adjusting sample interval and noise contributed by measurement uncertainty were computed by resampling from the 15-minute interval measurements made between May 1 2009 and May 1, 2012 and recomputing sand mass balances. The solid line is the SNR accounting for both noise sources.

Random selection from among the mapped segments results in a decrease in the standard deviation of the estimated sand budget as proportionally greater area is mapped (Figure 9(a)). Thus, SNR_{ms} associated with subsampling morphological measurements is a steep function of proportion that is sampled up to approximately 10% (Figure 9(b)). SNR_{ms} is a relatively shallow function of sampled proportion at intermediate sample sizes (from

approximately 10% to 85% of the reach sampled), and a steep function again for the remaining 15% (Figure 9(b)). When measurement uncertainty is neglected, the sand budget may be determined with $SNR_{ms} \geq 1$ with 10% of the area sampled and $SNR_{ms} \geq 2$ with 20% of the area sampled. However, the constant measurement uncertainty with $SNR_{mm} = 1.4$ limits the increase in total SNR_{mT} as the proportion of area sampled increases. When both measurement and subsampling noise are considered, at least 40–50% of the study area must be sampled to determine the sand budget with $SNR_{mT} \geq 1$, and $SNR_{mT} \geq 2$ could only be achieved by a decrease in measurement uncertainty.

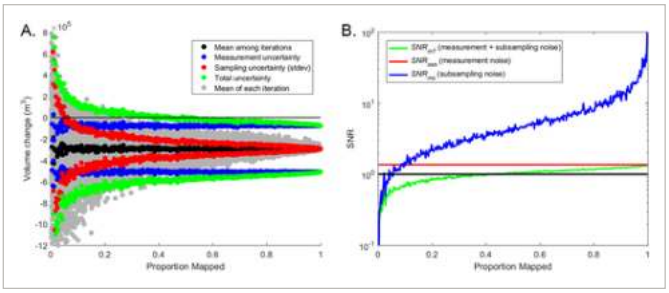

Figure 9

Open in figure viewer | PowerPoint

(A) Estimated morphological sand budget and uncertainties as functions of proportion of study area sampled. Because the simulation includes 100 iterations, the mean budget among iterations is approximately constant. The standard deviation among the iterations decreases as the proportion of the area sampled increases. Measurement uncertainty is constant relative to the mean volume changes. The total uncertainty is the sum of the measurement and sampling uncertainties and, therefore, approaches the value of the measurement uncertainty as sampling uncertainty decreases. (B) The signal-to-noise ratio (SNR) as a function of proportion of study segment mapped, distinguishing noise caused by sampling and noise caused by measurement uncertainty. The solid line is the SNR accounting for both noise sources.

Extrapolated morphological sand budget

Based on the average change in active deposits where measurements were made, we estimate an additional 110 800 ± 28 900 m^3 of net erosion from the active deposits in the remainder of the study area where measurements were not made (Table 4 and Figure 2). This produces an extrapolated net sand budget of –404 300 ± 219 700 m^3 (–642 900 ± 349 200 Mg), which results in substantially improved agreement with the flux-based sand budget. Although the uncertainty in the extrapolated budget is larger than in the budget without extrapolation, there is greater overlap between the uncertainty bands in the morphological and flux-based budgets (Figure 2).

Table 4. Extrapolated morphological sand budget

Measured sand budget (m^3)	-293,500±190,800
Measured area (m^2)	2,967,100
Mean change (m)	-0.10
Unmeasured active deposits (m^2)	1,120,617
Estimated change in unmeasured deposits (m^3)	-110,800±28,900
Extrapolated budget (m^3)	-404,300±219,700
Extrapolated budget (Mg)	-642,900±349,200

Discussion

Accurate sediment budgeting remains of paramount importance in regulated rivers, especially given the recent global trend in acceleration of new dam construction (Kondolf *et al*., 2014) as well as the acceleration in river restoration and dam removal projects in the United States (Bellmore *et al*., 2017). Numerous studies have documented that variations in the relative magnitudes of altered sediment-transport capacity and sediment-supply perturbation result in a continuum of effects downstream from large dams (Williams and Wolman, 1984; Andrews, 1986; Grant *et al*., 2003). While sediment deficit is common immediately downstream from dams (Draut *et al*., 2011; Ma *et al*., 2012), accumulation of tributary inputs can cause reversal to conditions of an indeterminate sediment budget or sediment surplus (Andrews, 1986; Schmidt and Wilcock, 2008). Such a range of conditions exist on the Colorado River downstream from Glen Canyon Dam (Schmidt and Wilcock, 2008), where estimates of the sand budget have been used to predict the long-term fate of alluvial sand deposits in lower Marble Canyon and other river segments within Grand Canyon for over 4 decades. Laursen *et al*. (1976) estimated the annual sand deficit was about 3 million Mg and predicted that progressive sand evacuation would lead to the eventual loss of most sandbars. In contrast, Howard and Dolan (1981) concluded that post-dam sand transport capacity, reduced without large annual snowmelt floods, would allow accumulation of sand in pools and eddies. This expectation of sand accumulation guided the release of the first controlled flood in 1996 (Webb *et al*., 1999). Observations made during and following the 1996 controlled flood of sand concentrations, sand grain sizes, and erosion of sand in eddies (Rubin *et al*., 1998; Topping *et al*., 1999; Hazel *et al*., 1999; Schmidt *et al*., 1999), coupled with detailed re-analysis of the historical record of suspended-sand loads (Topping *et al*., 2000a, b), provided evidence that sand did not typically accumulate in the channel for multi-year periods and that sand supply was likely declining (Hazel *et al*.,

1999; Schmidt, 1999; Rubin *et al*., 2002). Recent studies have presented evidence for sand accumulation in lower-discharge years in some reaches between 2002 and 2009 (Grams *et al*., 2013) and between 2012 and 2015 (Grams *et al*., 2015).

These sometimes-conflicting interpretations of the sand budget and associated implications for the long-term fate of sandbars stem from the combination of limited and temporally variable sand supply, a dam-altered flow regime with varying transport capacity, large uncertainty in the historical sand-transport data, and absence of robust morphological measurements. Because previous studies were either event-based (Webb *et al*., 1999) or relied on sparse data (Laursen *et al*., 1976; Howard and Dolan, 1981), reliable estimates for trends in sand storage over periods of many years have been elusive. Although the sand evacuation shown by this study applies only to a relatively short three-year period, it is the first study to rigorously quantify a segment-scale sand budget with well-constrained uncertainty. The difference between sand evacuation and accumulation has important management implications and could lead managers to consider adjustments in the magnitude, frequency, and timing of controlled floods. Application of the methods applied in this study over longer time periods will allow comparison among periods of evacuation, accumulation, and stability to produce more robust predictions of the long-term fate of sandbars in Grand Canyon.

Floods from the Paria River comprise approximately 90% of the annual sand supply to the Colorado River upstream from lower Marble Canyon and downstream from Glen Canyon Dam (Griffiths and Topping, 2017) and can result in the accumulation of up to 2 million Mg of sand in in some years (Grams *et al*., 2015). However, inputs in many years are much less and the average annual sand supply from this tributary was 544 000 Mg during the 3-year study period (Figure 2). Thus, the ~500 000 Mg ± 300 000 Mg of sand evacuation we measured is a substantial proportion of that supply. The erosion that occurred in just a few months in 2011 created a deficit that requires a large fraction of the average annual inputs to replenish. Sequential periods of depletion of this magnitude would, therefore, have a major impact on the long-term sand budget. Although the sand evacuation measured during this study is the largest that has occurred since the current high-resolution sand flux monitoring program was initiated in 2002 (Topping and Wright, 2016), it was preceded by periods of erosion that were likely larger. Based on analysis of suspended sediment records, Topping *et al*. (2003) estimated that about 16 million Mg of sand, silt and clay was eroded from the segment between Lees Ferry and Rkm 140 during a series of high-flow pulses during 1965. Grain-size analyses of a subset of the daily suspended-sediment samples indicate that most of this 16 million Mg was sand (US Geological Survey, 1970). Further, at least two million Mg of sand, and likely much more, were eroded from Marble Canyon during a series of scouring events that occurred from 1997 to 2000 resulting in substantial sandbar erosion (Rubin *et al*., 2002).

Even with state-of-the-art measurement capabilities such as those applied in this study, uncertainty in measurements of sand flux or morphological change can be substantial. Uncertainty of only a few percent in measurements of sand flux accumulate in time and, in the case of lower Marble Canyon, may become larger than budget signal within only 3 to 10 years. Similarly, we have shown that uncertainty of only a few centimeters in individual morphological measurements accumulates to a very large volume when the region of interest is many km in length. Despite finding no comparable reporting of uncertainty in volumetric changes associated with coincident measurements of bed-sediment composition, and with potential changes in unmeasured areas, in the literature, the estimates of uncertainty we used for individual morphological measurements (4 to 12 cm) are consistent with the magnitude of uncertainty involved in other high-resolution mapping methods (Williams *et al*., 2014; Schimel *et al*., 2015; Passalacqua *et al*., 2015). In measurements of sediment flux, uncertainty cannot be less than the uncertainty in measurements of discharge, which are typically considered to be ± 3% to ± 5% for “excellent” records (Rantz *et al*., 1982). When these major sources of uncertainty are fully considered, uncertainty in sediment budgets that is similar to or greater than the budget signal is common (Erwin *et al*., 2012; Grams *et al*., 2013; Schaffrath *et al*., 2015; Warrick *et al*., 2015). For these reasons, the agreement (within uncertainty) of two entirely independent measurements for change in sand storage provides valuable verification that the measured signal is correct.

The problem of large uncertainty and low SNR is compounded when the sampling design does not adequately account for temporal and spatial variability in sediment flux and morphological change. In this study, low SNR is dictated by large temporal/spatial scales (i.e. large noise) and small upstream sand supply (i.e. small signal) acting in concert. These findings have direct relevance to other large dammed rivers with marginal sand inputs from tributaries, and for rivers with sediment bypass systems designed to mitigate sediment starvation downstream of reservoirs (Kondolf *et al*., 2014). We argue that the SNR framework is a useful and adaptable approach to evaluate sampling design and quantify the sampling required to maximize SNR, and the minimal sampling that equates to an acceptably high SNR.

In the flux-based budget, as noise caused by subsampling increases, SNR_{fs} decays exponentially as a function of increasing sample interval (Figure 8). For the lower Marble Canyon data, accounting for both the noise contributed by adjusting sample interval and the noise contributed by measurement uncertainty (i.e. the solid line in Figure 8), the SNR_{fT} falls below 1 at sample intervals greater than 2 days. Noise in this case is quantified as the standard deviation of subsampled records of discharge and SSC, and the increase in this quantity is the result of physical processes that cause sub-daily variations in SSC, such as changes in sand supply or bed configuration (Topping and Wright, 2016). Considering both sources of noise (measurement plus subsampling), sampling at least every other day is required to determine the sand budget $SNR_{fT} \geq 1$), and sub-daily sampling for $SNR_{fT} \geq 2$. This is a much more frequent sample interval than the 10 to 12 sample per year frequency that Horowitz *et al*. (2015) suggested was required to estimate annual suspended-sediment loads. However, the lowest sample frequency considered by Horowitz *et al*. (2015) was 1 day and their evaluation criteria was the sample interval required to estimate annual loads within 20% of the annual load determined by daily sampling. Their analysis, therefore, ignored the effect of measurement uncertainty on the cumulative load and considered the annual load determined by daily sampling as the ‘true’ annual load. Our SNR analysis considers both measurement error and sampling bias, down to sub-hourly sample intervals. Considering only the noise contributed by the sampling interval (i.e. the dotted blue line in Figure 8), SNR_{fs} crosses 1 at a sample interval of 10 days, which is in somewhat closer agreement with the finding of Horowitz *et al*. (2015). This example clearly illustrates the importance of considering both measurement and sampling uncertainty in sampling design. Neglecting either source of uncertainty will likely result in undersampling and an underestimation of uncertainty. In addition, our goal of achieving $SNR_{fT} \geq 1$ is different from the objective of estimating an annual load to within 20%. Although there may be cases where estimation of annual loads within 20% is acceptable, that level of uncertainty will likely result in indeterminate sediment budgets, unless the erosional or depositional signal is very large.

The SNR analysis of the morphological sand budget indicates that measurement noise is a larger contributor to overall uncertainty than spatial variability in erosion and deposition patterns, despite the significant heterogeneity in the latter. Further, the analysis suggests that data from 50% or more of the segment of interest must be utilized to determine the sand budget with $SNR_{mT} \geq 1$, when sampling and measurement uncertainty are both considered (Figure 9(b)). Although sampling uncertainty contributes substantially to the total uncertainty, measurement uncertainty places a severe upper limit on SNR_{mT}. Thus, unless measurement uncertainty can be reduced, very robust spatial sampling is required to determine the sand budget. Comprehensive spatial sampling is, however, rarely possible in large rivers. Even using advanced mapping methods, we were able to determine morphological changes for only 71% of the active channel within the study area. Nevertheless, simulation of the effect of decreasing sample coverage with the available measurements in the SNR analysis provides a framework for extrapolation of the budget to unmeasured areas. This application of the SNR is based on the assumption that the distribution of morphological changes in the ~30% of the segment we did not map can be approximated by the distribution of the changes that were measured. Because measurements were made throughout the study area and the only areas systematically avoided were cobble- and boulder-bedded rapids and riffles, this assumption is reasonable.

Despite much emphasis on measurement uncertainty (Wheaton *et al*., 2010; Bangen *et al*., 2016) associated with high-resolution mapping (Williams *et al*., 2014) and high-resolution measurements of sediment flux (Topping *et al*., 2010; Topping and Wright, 2016), these results demonstrate that noise generated through undersampling may, in some cases, outweigh measurement error and should be incorporated in sampling design and quantification of uncertainty. Because the relations between sample density and noise presented in this study are based on high-resolution data collected in a particular setting, the values for required minimum sample interval or minimum proportion of study reach that must be measured are specific to this study. Indeed, we have demonstrated that the sampling-related uncertainty depends on physical processes that cause temporal variability in sediment transport and spatial variability in morphological change, which are expected to vary among river systems. Nevertheless, temporally-variable sediment flux is not uncommon, and flux measurements with high temporal density are likely required to develop accurate sand budgets across a wide range of river systems. This is reflected by the increasing popularity of surrogate methods, such as acoustical techniques, that allow measuring sediment concentration at high sample frequency (Moore *et al*., 2012; Sassi *et al*., 2012; Dean *et al*., 2016; Haught *et al*., 2017). Similarly, spatially-variable sedimentation is also common and repeat mapping of the majority of a river segment is also likely required for many river systems.

Collection of similar data for longer periods and in other settings is required to evaluate the degree to which the relations found here vary among river systems. The flux and morphological mass balance estimation, uncertainty quantification, and techniques for including both measurement and sampling uncertainty in a SNR estimate presented here may be reproduced for other rivers whose transport is dominated by sand and where there is temporal variation in sediment supply and/or spatial variability in erosion and deposition. It is likely that similar relations will be found that could be used to refine sampling guidelines, which may vary among river systems. For example, the curve shown in Figure 9 would be expected to shift to the right or left if morphological changes are more or less localized than we observed, respectively. These tools to evaluate the effects of sampling frequency and spatial extent on the accuracy of sediment budgets and the meaningful detection of morphological change should be applied in the design of both short- and long-term studies; and thereby improve evaluations of the potential impacts of water developments, other engineering structures designed to store or redistribute water and/or sediment, or climate and land-use changes.

Conclusions

Complementary measurements of sand transport and morphological change were used to compute a segment-scale (>100 channel widths) sand budget for lower Marble Canyon, a 50-km segment of the Colorado River in Grand Canyon National Park. The river flows within a debris-fan dominated canyon in which sediment-storage locations are hydraulically forced by tributary debris fans. The flux-based sand budget was computed from continuous (15-minute) measurements of suspended-sand transport at the upstream and downstream ends of the study area. The morphological sand budget was computed from two surveys using multibeam sonar, singlebeam sonar, and conventional topographic surveys conducted in May 2009 and May 2012. These entirely independent methods for computing the sand budget agree within a conservative estimate of uncertainty and the flux-based sand budget indicates 702 000 ± 317 000 Mg of erosion for the 3-year study period.

According to the flux-based sand budget, almost all of the sand evacuation from the study area occurred during a 7-month period of high dam release volumes in 2011. The morphological measurements reveal the spatial distribution of those changes and show that approximately 70% of the net volume of sand evacuation occurred in specific geomorphic settings that occupied less than 12% of the study segment by area. The magnitude of morphological change was controlled by depositional setting. Eddies were the most morphologically active depositional setting, but did not experience net erosion. Large pools and scour holes in the main channel adjacent to eddies were the primary source of the eroded sand.

A novel aspect of the sand budget was the incorporation of high-resolution bed-sediment classifications using multibeam acoustic backscatter, which show that approximately 80–90% of the bed in eddies and 50–70% of the bed of the river in the main channel is composed of sand, and allowed estimation of elevation uncertainties in the remaining graveled or rocky portions of the bed. The proportion of the bed composed of sand decreased by less than 8% between May 2009 and May 2012, and this decrease occurred primarily by changes from sand to rock or gravel around the edges of sand patches in the channel. Very few contiguous patches of sand were eroded to expose gravel, indicating that, during this erosion event, most of the change in sand storage occurred by changes in the thickness of sand deposits within the river bed rather than by large spatial redistributions of surficial sand.

A signal-to-noise analysis of potential systematic errors in the sand mass balances indicated that noise generated through undersampling of either sediment flux or morphological change may exceed noise contributed by measurement error. For the Colorado River in Grand Canyon, daily sampling of suspended-sand concentration is required to determine the sand budget with $SNR_{fT} \geq 1$, and sub-daily sampling is required to achieve $SNR_{fT} \geq 2$. Signal-to-noise analysis of repeat morphological measurements indicates that at least 50% of the segment must be mapped to estimate the budget with $SNR_{mT} \geq 1$. Achievement of $SNR_{mT} \geq 2$ would require substantial reduction in measurement uncertainty in concert with robust spatial sampling. The SNR analysis of the influence of the spatial extent of morphological measurements on the sand budget was also used to extrapolate the morphological budget to regions in the study area where morphological data were not collected, which resulted in improved agreement with the flux-based sand budget. The effects of

sampling frequency and spatial extent on the accuracy of sediment budgets and the detection of significant morphological change should be carefully considered in the design of both short- and long-term fluvial sedimentation studies.

Acknowledgements

This study was funded by the Glen Canyon Dam Adaptive Management Program administered by the US Department of the Interior Bureau of Reclamation. The authors acknowledge the contributions of the many scientists, field technicians, and river guides who have dedicated themselves to the study of the Colorado River in Grand Canyon. In particular, Daniel Hadley, Daniel Hamill, Keith Kohl, Erich Mueller, Robert Ross, and Robert Tusso made substantial contributions to data collection and processing. Jonathan Warrick, Amanda Schmidt, Susannah Erwin, and two anonymous reviewers provided thorough and constructive comments on previous drafts of this manuscript that are gratefully acknowledged. Any use of trade, product, or firm names is for descriptive purposes only and does not imply endorsement by the US Government.

Supporting Information

esp4489-sup-0001-supporting_info.tiff TIFF image, 149 KB	**Figure S1**. Distribution of fiducial polygon errors. The error for each fiducial polygon error was calculated as the difference in mean elevation between the 2009 and 2012 DEMs. The mean signed error among all 79 polygons was –0.01 m with standard deviation of 0.03 m and mean absolute error of 0.02 m.
esp4489-sup-0002-supporting_info.tif TIFF image, 1.6 MB	**Figure S2.** The mean error, mean absolute error, and standard deviation as a function of the extent of fiducial regions sampled. The extent sampled was varied by randomly selecting the required number of 1-m^2 pixels from within all fiducial regions in each of the 44 survey segments (each ~1 km in length) distributed throughout the study area.

Please note: The publisher is not responsible for the content or functionality of any supporting information supplied by the authors. Any queries (other than missing content) should be directed to the corresponding author for the article.

Andermann C, Crave A, Gloaguen R, Davy P, Bonnet S. 2012. Connecting source and transport: suspended sediments in the Nepal Himalayas. *Earth and Planetary Science Letters* **351–352**: 158– 170. https://doi-org.libproxy.nau.edu/10.1016/j.epsl.2012.06.059 .
Crossref | CAS | ADS | Web of Science® | Google Scholar | FullText@NAU

Andrews ED. 1986. Downstream effects of Flaming Gorge Reservoir on the Green River, Colorado and Utah. *Geological Society of America Bulletin* **97**: 1012–1023. https://doi-org.libproxy.nau.edu/10.1130/0016-7606(1986)97<1012 .
Crossref | ADS | Web of Science® | Google Scholar | FullText@NAU

Ashworth PJ, Best JL, Bristow CS. 2000. Morphological evolution and dynamics of a large, sand braid-bar, Jamuna River, Bangladesh. *Sedimentology* **47**: 533– 555. https://doi-org.libproxy.nau.edu/10.1046/j.1365-3091.2000.00305.x .
Wiley Online Library | Web of Science® | Google Scholar | FullText@NAU

Bangen S, Hensleigh J, McHugh P, Wheaton J. 2016. Error modeling of DEMs from topographic surveys of rivers using fuzzy inference systems. *Water Resources Research* **52**: 1176– 1193. https://doi-org.libproxy.nau.edu/10.1002/2015WR018299 .
Wiley Online Library | ADS | Web of Science® | Google Scholar | FullText@NAU

Bellmore RJ, Duda JJ, Craig LS, Greene SL, Torgersen CE, Collins MJ, Vittum K. 2017. Status and trends of dam removal research in the United States. *Wiley Interdisciplinary Reviews: Water* **4**: e1164. https://doi-org.libproxy.nau.edu/10.1002/wat2.1164 .
Wiley Online Library | Web of Science® | Google Scholar | FullText@NAU

Belmont P, Gran KB, Schottler SP, Wilcock PR, Day SS, Jennings C, Lauer JW, Viparelli E, Willenbring JK, Engstrom DR, Parker G. 2011. Large shift in source of fine sediment in the upper Mississippi river. *Environmental Science and Technology* **45**: 8804– 8810. https://doi-org.libproxy.nau.edu/10.1021/es2019109 .
Crossref | CAS | ADS | PubMed | Web of Science® | Google Scholar | FullText@NAU

Brasington J, Rumsby BT, McVey RA. 2000. Monitoring and modelling morphological change in a braided gravel-bed river using high resolution GPS-based survey. *Earth Surface Processes and Landforms* **25**: 973– 990. https://doi-org.libproxy.nau.edu/10.1002/1096-9837(200008)25:9<973::AID-ESP111>3.0.CO;2-Y .
Wiley Online Library | ADS | Web of Science® | Google Scholar | FullText@NAU

Brock JC, Sallenger AH, Krablll WB, Swift RN, Wrlght CW. 2001. Recognition of fiducial surfaces in Lidar surveys of coastal topography. *Photogrammetric Engineering and Remote Sensing* **67**: 1245– 1258.
Web of Science® | Google Scholar | FullText@NAU

Buscombe D. 2013. Transferable wavelet method for grain-size distribution from images of sediment surfaces and thin sections, and other natural granular patterns. *Sedimentology* **60**: 1709– 1732. https://doi-org.libproxy.nau.edu/10.1111/sed.12049 .
Wiley Online Library | Web of Science® | Google Scholar | FullText@NAU

Buscombe D, Grams PE, Kaplinski MA. 2014a. Characterizing riverbed sediment using high-frequency acoustics: 1. Spectral properties of scattering. *Journal of Geophysical Research: Earth Surface* **119**: 2674– 2691. https://doi-org.libproxy.nau.edu/10.1002/2014JF003189 .
Wiley Online Library | ADS | Web of Science® | Google Scholar | FullText@NAU

Buscombe D, Grams PE, Kaplinski MA. 2014b. Characterizing riverbed sediment using high-frequency acoustics: 2. Scattering signatures of Colorado River bed sediment in Marble and Grand Canyons. *Journal of Geophysical Research: Earth Surface* **119**: 2692– 2710 https://doi-org.libproxy.nau.edu/10.1002/2014JF003191.In .
Wiley Online Library | ADS | Web of Science® | Google Scholar | FullText@NAU

Buscombe D, Grams PE, Kaplinski MA. 2017. Compositional signatures in acoustic backscatter over vegetated and unvegetated mixed sand-gravel riverbeds. *Journal of Geophysical Research: Earth Surface* **122**: 1– 23. https://doi-org.libproxy.nau.edu/10.1002/2017JF004302 .
Wiley Online Library | Google Scholar | FullText@NAU

Cohn TA. 1995. Recent advances in statistical methods for the estimation of sediment and nutrient transport in rivers. *Reviews of Geophysics* **33**: 1117– 1123. https://doi-org.libproxy.nau.edu/10.1029/95RG00292 .
Wiley Online Library | ADS | Web of Science® | Google Scholar | FullText@NAU

Colby BR. 1964. Scour and Fill in Sand-Bed Streams. US Geological Survey Professional Paper 462-D: 39. [online] Available from: https://pubs.er.usgs.gov/publication/pp462D
Google Scholar | FullText@NAU

Cover TM, Thomas JA. 1991. *Elements of Information Theory*. John Wiley and Sons: New York, NY.
Wiley Online Library | Google Scholar | FullText@NAU

Curry CW, Bennett RH, Hulbert MH, Curry KJ. 2004. Comparative study of sand porosity and a technique for determining porosity of undisturbed marine sediment. *Marine Georesources and Geotechnology* **22**: 231– 252. https://doi-org.libproxy.nau.edu/10.1080/10641190490900844 .
Crossref | CAS | Web of Science® | Google Scholar | FullText@NAU

Davis PA. 2012. Airborne Digital-Image Data for Monitoring the Colorado River Corridor below Glen Canyon Dam, Arizona, 2009 — Image-Mosaic Production and Comparison with 2002 and 2005 Image Mosaics. US Geological Survey Open-File Report 2012-1139: 82. [online] Available from: http://pubs.usgs.gov/of/2012/1139/
Google Scholar | FullText@NAU

Dean DJ, Topping DJ, Schmidt JC, Griffiths RE, Sabol TA. 2016. Sediment supply versus local hydraulic controls on sediment transport and storage in a river with large sediment loads. *Journal of Geophysical Research: Earth Surface* **121**: 82– 110. https://doi-org.libproxy.nau.edu/10.1002/2015JF003436 .
Wiley Online Library | ADS | Web of Science® | Google Scholar | FullText@NAU

Dinehart RL. 1998. Sediment transport at gaging stations near Mount St. Helens, Washington, 1980–1990. US Geological Survey Professional Paper 1573: 105. Available from: https://pubs.usgs.gov/pp/1573/
Google Scholar | FullText@NAU

Draut AE. 2012. Effects of river regulation on aeolian landscapes, Colorado River, southwestern USA. *Journal of Geophysical Research* **117**: F02022. https://doi-org.libproxy.nau.edu/10.1029/2011JF002329 .
Wiley Online Library | Web of Science® | Google Scholar | FullText@NAU

Draut AE, Logan JB, Mastin MC. 2011. Channel evolution on the dammed Elwha River, Washington, USA. *Geomorphology* **127**: 71– 87. https://doi-org.libproxy.nau.edu/10.1016/j.geomorph.2010.12.008 .
Crossref | ADS | Web of Science® | Google Scholar | FullText@NAU

Erwin SO, Schmidt JC, Wheaton JM, Wilcock PR. 2012. Closing a sediment budget for a reconfigured reach of the Provo River, Utah, United States. *Water Resources Research* **48**: W10512. https://doi-org.libproxy.nau.edu/10.1029/2011WR011035 .
Wiley Online Library | ADS | Web of Science® | Google Scholar | FullText@NAU

Ferguson RI. 1986. River loads underestimated by rating curves. *Water Resources Research* **22**: 74– 76. https://doi-org.libproxy.nau.edu/10.1029/WR022i001p00074 .
Wiley Online Library | CAS | ADS | Web of Science® | Google Scholar | FullText@NAU

Grams PE, Schmidt JC. 2005. Equilibrium or indeterminate? Where sediment budgets fail: sediment mass balance and adjustment of channel form, Green River downstream from Flaming Gorge Dam, Utah and Colorado. *Geomorphology* **71**: 156– 181. https://doi-org.libproxy.nau.edu/10.1016/j.geomorph.2004.10.012 .
Crossref | ADS | Web of Science® | Google Scholar | FullText@NAU

Grams PE, Schmidt JC, Wright SA, Topping DJ, Melis TS, Rubin DM. 2015. Building sandbars in the Grand Canyon. *EOS, Transactions American Geophysical Union* **96**: 12– 16. https://doi-org.libproxy.nau.edu/10.1029/2015EO030349 .
Crossref | Google Scholar | FullText@NAU

Grams PE, Topping DJ, Schmidt JC, Hazel JE Jr, Kaplinski M. 2013. Linking morphodynamic response with sediment mass balance on the Colorado River in Marble Canyon: issues of scale, geomorphic setting, and sampling design. *Journal of Geophysical Research: Earth Surface* **118**: 21. https://doi-org.libproxy.nau.edu/10.1002/jgrf.20050 .
Wiley Online Library | Google Scholar | FullText@NAU

Grant GE, Schmidt JC, Lewis SL. 2003. A geological framework for interpreting downstream effects of dams on rivers. In *A Peculiar River*, JE O'Connor, GE Grant (eds). American Geophysical Union: Where?; 203– 219. https://doi-org.libproxy.nau.edu/10.1029/007WS13
Wiley Online Library | Web of Science® | Google Scholar | FullText@NAU

Griffiths RE, Topping DJ. 2017. Importance of measuring discharge and sediment transport in lesser tributaries when closing sediment budgets. *Geomorphology* **296**: 59–73. https://doi-org.libproxy.nau.edu/10.1016/j.geomorph.2017.08.037 .
Crossref | ADS | Web of Science® | Google Scholar | FullText@NAU

Griffiths RE, Topping DJ, Andrews T, Bennet GE, Sabol TA, Melis TS. 2012. Design and maintenance of a network for collecting high-resolution suspended-sediment data at remote locations on rivers, with examples from the Colorado River. *US Geological Survey Techniques and Methods* **8**(44) [online] Available from: https://pubs.usgs.gov/tm/tm8c2/ .
Google Scholar | FullText@NAU

Haught D, Venditti JG, Wright SA. 2017. Calculation of *in situ* acoustic sediment attenuation using off-the-shelf horizontal ADCPs in low concentration settings. *Water Resources Research*. https://doi-org.libproxy.nau.edu/10.1002/2016WR019695 .
Wiley Online Library | Web of Science® | Google Scholar | FullText@NAU

Hazel JE Jr, Kaplinski M, Parnell RA, Kohl K, Schmidt JC. 2008. Monitoring fine-grained sediment in the Colorado River Ecosystem, Arizona – control network and conventional survey techniques. *US Geological Survey Open-File Report* **2008–1276**: 15 Available from: https://pubs.usgs.gov/of/2008/1276/ .
Google Scholar | FullText@NAU

Hazel JE Jr, Grams PE, Schmidt JC, Kaplinski M. 2010. Sandbar response following the 2008 high-flow experiment on the Colorado River in Marble and Grand Canyons. US Geological Survey Scientific Investigations Report 2010–5015: 52. [online] Available from: http://pubs.usgs.gov/sir/2010/5015
Google Scholar | FullText@NAU

Hazel JE Jr, Kaplinski M, Parnell R, Manone M, Dale A. 1999. Topographic and bathymetric changes at thirty-three long-term study sites. In *The Controlled Flood in Grand Canyon*, RH Webb, JC Schmidt, RA Valdez, GR Marzolf (eds). American Geophysical Union: Where?; 161– 183. https://doi-org.libproxy.nau.edu/10.1029/GM110p0161
Wiley Online Library | Google Scholar | FullText@NAU

Hazel JE Jr, Topping DJ, Schmidt JC, Kaplinski M. 2006. Influence of a dam on fine-sediment storage in a canyon river. *Journal of Geophysical Research* **111**: F01025. https://doi-org.libproxy.nau.edu/10.1029/2004JF000193 .
Wiley Online Library | ADS | Web of Science® | Google Scholar | FullText@NAU

Hinderer M. 2012. From gullies to mountain belts: a review of sediment budgets at various scales. *Sedimentary Geology* **280**: 21– 59. https://doi-org.libproxy.nau.edu/10.1016/j.sedgeo.2012.03.009 .
Crossref | ADS | Web of Science® | Google Scholar | FullText@NAU

Hoffmann T, Thorndycraft VR, Brown AG, Coulthard TJ, Damnati B, Kale VS, Middelkoop H, Notebaert B, Walling DE. 2010. Human impact on fluvial regimes and sediment flux during the Holocene: review and future research agenda. *Global and Planetary Change* **72**: 87– 98. https://doi-org.libproxy.nau.edu/10.1016/j.gloplacha.2010.04.008 .
Crossref | ADS | Web of Science® | Google Scholar | FullText@NAU

Hooke JM. 2007. Spatial variability, mechanisms and propagation of change in an active meandering river. *Geomorphology* **84**: 277– 296. https://doi-org.libproxy.nau.edu/10.1016/j.geomorph.2006.06.005 .
Crossref | ADS | Web of Science® | Google Scholar | FullText@NAU

Horowitz AJ, Clarke RT, Merten GH. 2015. The effects of sample scheduling and sample numbers on estimates of the annual fluxes of suspended sediment in fluvial systems. *Hydrological Processes* **29**: 531– 543. https://doi-org.libproxy.nau.edu/10.1002/hyp.10172 .
Wiley Online Library | ADS | Web of Science® | Google Scholar | FullText@NAU

Howard A, Dolan R. 1981. Geomorphology of the Colorado River in the Grand Canyon. *The Journal of Geology* **89**: 269– 298. https://doi-org.libproxy.nau.edu/10.1086/628592 .
Crossref | ADS | Web of Science® | Google Scholar | FullText@NAU

James LA, Hodgson ME, Ghoshal S, Latiolais MM. 2012. Geomorphic change detection using historic maps and DEM differencing: the temporal dimension of geospatial analysis. *Geomorphology* **137**: 181– 198. https://doi-org.libproxy.nau.edu/10.1016/j.geomorph.2010.10.039 .
Crossref | ADS | Web of Science® | Google Scholar | FullText@NAU

Julien PY, Klaassen GJ, Ten Brinke WBM, Wilbers AWE. 2002. Case study: bed resistance of Rhine river during 1998 flood. *Journal of Hydraulic Engineering* **128**: 1042– 1050. https://doi-org.libproxy.nau.edu/10.1061/(ASCE)0733-9429(2002)128:12(1042) .
Crossref | Web of Science® | Google Scholar | FullText@NAU

Kaplinski M, Grams PE, Hazel JE, Jr, Buscombe D, Kohl K, Hensleigh J. 2018. Channel Mapping of the Colorado River in Grand Canyon National Park, Arizona - May 2012, river miles 29 to 62–Data: U.S. *Geological Survey data release*, https://dx-doi-org.libproxy.nau.edu/10.5066/P9CIMU68
Google Scholar | FullText@NAU

Kaplinski M, Hazel JE Jr, Grams PE, Davis PA. 2014. Monitoring fine-sediment volume in the Colorado river ecosystem, Arizona – construction and analysis of digital elevation models. *US Geological Survey Open-file Report* 20141052: 36. https://doi-org.libproxy.nau.edu/10.3133/ofr20141052
Google Scholar | FullText@NAU

Kaplinski M, Hazel JE Jr, Grams PE, Kohl K, Buscombe DD, Tusso RB. 2017a. Channel mapping of the Colorado river in Grand Canyon National Park, Arizona – May 2009, river miles 29 to 62 – Data. *US Geological Survey data release.* https://doi-org.libproxy.nau.edu/10.5066/F7930RCG .
Google Scholar | FullText@NAU

Kaplinski M, Hazel JE, Jr, Grams PE, Kohl K, Buscombe DD, Tusso RB. 2017b. Channel Mapping River Miles 29–62 of the Colorado River in Grand Canyon National Park, Arizona, May 2009. US Geological Survey Open-File Report 2017–1030*DOI* https://doi-org.libproxy.nau.edu/10.3133/ofr20171030 .
Google Scholar | FullText@NAU

Kearsley LH, Schmidt JC, Warren KD. 1994. Effects of Glen Canyon Dam on Colorado River sand deposits used as campsites in Grand Canyon National Park, USA. *Regulated Rivers* **9**: 137– 149. https://doi-org.libproxy.nau.edu/10.1002/rrr.3450090302 .
Wiley Online Library | Web of Science® | Google Scholar | FullText@NAU

Kiang J, Cohn T, Mason R. 2016. A survey of the uncertainty in stage-discharge rating curves and streamflow records in the United States. In *River Flow 2016, Proceedings of the International Conference on Fluvial Hydraulics*, G Constantinescu, M Garcia, D Hanes (eds): CRC Press St. Louis, Missouri.
Crossref | Google Scholar | FullText@NAU

Kleinhans MG, Wilbers AWE, ten Brinke WBM. 2007. Opposite hysteresis of sand and gravel transport upstream and downstream of a bifurcation during a flood in the Rhine River, the Netherlands. *Netherlands Journal of Geosciences* **86**: 273– 285 [online] Available from: https://dspace.library.uu.nl/handle/1874/40663 .
Crossref | Web of Science® | Google Scholar | FullText@NAU

Kondolf GM, Matthews WVG. 1991. Unmeasured residuals in sediment budgets: a cautionary note. *Water Resources Research* **27**: 2483– 2486.
https://doi-org.libproxy.nau.edu/10.1029/91WR01625 .
Wiley Online Library | ADS | Web of Science® | Google Scholar | FullText@NAU

Kondolf GM, Gao Y, Annandale GW, Morris GL, Jiang E, Zhang J, Cao Y, Carling P, Fu K, Guo Q, Hotchkiss R, Peteuil C, Sumi T, Wang H, Wang Z, Wei Z, Wu B, Wu C, Yang CT. 2014. Sustainable sediment management in reservoirs and regulated rivers: experiences from five continents. *Earth's Future* **2**: 256– 280.
https://doi-org.libproxy.nau.edu/10.1002/2013EF000184 .
Wiley Online Library | ADS | Web of Science® | Google Scholar | FullText@NAU

Korup O. 2012. Earth's portfolio of extreme sediment transport events. *Earth-Science Reviews* **112**: 115– 125.
https://doi-org.libproxy.nau.edu/10.1016/j.earscirev.2012.02.006 .
Crossref | ADS | Web of Science® | Google Scholar | FullText@NAU

Lane SN, Richards KS, Chandler JH. 1994. Developments in monitoring and modelling small-scale river bed topography. *Earth Surface Processes and Landforms* **19**(4): 349–368 https://doi-org.libproxy.nau.edu/10.1002/esp.3290190406 .
Wiley Online Library | ADS | Web of Science® | Google Scholar | FullText@NAU

Lane SN, Westaway RM, Hicks DM. 2003. Estimation of erosion and deposition volumes in a large, gravel-bed, braided river using synoptic remote sensing. *Earth Surface Processes and Landforms* **28**: 249– 271. https://doi-org.libproxy.nau.edu/10.1002/esp.483 .
Wiley Online Library | ADS | Web of Science® | Google Scholar | FullText@NAU

Laursen EM, Ince S, Pollack J. 1976. On sediment transport through the Grand Canyon. Proceedings of the Third Federal Interagency Sedimentation Conference: Denver, Colorado; 87.
Google Scholar | FullText@NAU

López-Tarazón JA, Batalla RJ, Vericat D, Francke T. 2012. The sediment budget of a highly dynamic mesoscale catchment: the River Isbena. *Geomorphology* **138**: 15– 28.
https://doi-org.libproxy.nau.edu/10.1016/j.geomorph.2011.08.020 .
Crossref | ADS | Web of Science® | Google Scholar | FullText@NAU

Ma Y, Huang HQ, Nanson GC, Li Y, Yao W. 2012. Channel adjustments in response to the operation of large dams: the upper reach of the lower Yellow River. *Geomorphology* **147–148**: 35– 48. https://doi-org.libproxy.nau.edu/10.1016/J.GEOMORPH.2011.07.032 .
Crossref | ADS | Web of Science® | Google Scholar | FullText@NAU

McLean DG, Church M. 1999. Sediment transport along lower Fraser River: 2. Estimates based on the long-term gravel budget. *Water Resources Research* **35**: 2549– 2559.
https://doi-org.libproxy.nau.edu/10.1029/1999WR900102 .
Wiley Online Library | ADS | Web of Science® | Google Scholar | FullText@NAU

Moore SA, Le Coz J, Hurther D, Paquier A. 2012. On the application of horizontal ADCPs to suspended sediment transport surveys in rivers. *Continental Shelf Research* **46**: 50– 63. https://doi-org.libproxy.nau.edu/10.1016/j.csr.2011.10.013 .
Crossref | ADS | Web of Science® | Google Scholar | FullText@NAU

Nichols KK, Bierman PR, Caffee M, Finkel R, Larsen J. 2005. Cosmogenically enabled sediment budgeting. *Geology* **33**: 133– 136.
https://doi-org.libproxy.nau.edu/10.1130/G21006.1 .
Crossref | ADS | Web of Science® | Google Scholar | FullText@NAU

Owens PN, Batalla RJ, Collins AJ, Gomez B, Hicks DM, Horowitz AJ, Kondolf GM, Marden M, Page MJ, Peacock DH, Petticrew EL, Salomons W, Trustrum NA. 2005. Fine-grained sediment in river systems: environmental significance and management issues. *River Research and Applications* **21**: 693– 717.
https://doi-org.libproxy.nau.edu/10.1002/rra.878 .
Wiley Online Library | Web of Science® | Google Scholar | FullText@NAU

Passalacqua P, Belmont P, Staley DM, Simley JD, Arrowsmith JR, Bode CA, Crosby C, DeLong SB, Glenn NF, Kelly SA, Lague D, Sangireddy H, Schaffrath K, Tarboton DG, Wasklewicz T, Wheaton JM. 2015. Analyzing high resolution topography for advancing the understanding of mass and energy transfer through landscapes: a review. *Earth-Science Reviews* **148**: 174– 193. https://doi-org.libproxy.nau.edu/10.1016/j.earscirev.2015.05.012 .
Crossref | ADS | Web of Science® | Google Scholar | FullText@NAU

Piégay H, Hicks DM. 2005. Sediment management in river systems: a need to assess changing processes in the long term and at a large scale. *River Research and Applications* **21**: 689– 691. https://doi-org.libproxy.nau.edu/10.1002/rra.877 .
Wiley Online Library | Web of Science® | Google Scholar | FullText@NAU

Pizzuto JE. 1994. Channel adjustments to changing discharges, Powder River, Montana. *Geological Society of America Bulletin* **106**: 1494– 1501.
https://doi-org.libproxy.nau.edu/10.1130/0016-7606(1994)106<1494:CATCDP>2.3.CO;2 .
Crossref | ADS | Web of Science® | Google Scholar | FullText@NAU

Porterfield G. 1972. Computation of Fluvial-Sediment Discharge. Techniques of Water-Resources Investigations of the United States Geological Survey, Book 3: 71. [online] Available from: https://pubs.usgs.gov/twri/twri3-c3/
Google Scholar | FullText@NAU

Rantz SE. 1982. Measurement and computation of streamflow: Volume 1. Measurement of Stage and Discharge. US Geological Survey Water Supply Paper 2175: 313. [online] Available from: https://pubs.usgs.gov/wsp/wsp2175/
Google Scholar | FullText@NAU

Rubin DM, Chezar H, Harney JN, Topping DJ, Melis TS, Sherwood CR. 2007. Underwater microscope for measuring spatial and temporal changes in bed-sediment grain size. *Sedimentary Geology* **202**: 402– 408. https://doi-org.libproxy.nau.edu/10.1016/j.sedgeo.2007.03.020 .
Crossref | ADS | Web of Science® | Google Scholar | FullText@NAU

Rubin DM, Nelson JM, Topping DJ. 1998. Relation of inversely graded deposits to suspended-sediment grain-size evolution during the 1996 flood experiment in Grand Canyon. *Geology* **26**: 99– 102. https://doi-org.libproxy.nau.edu/10.1130/0091-7613(1998)026<0099:ROIGDT>2.3.CO;2 .
Crossref | ADS | Web of Science® | Google Scholar | FullText@NAU

Rubin DM, Schmidt JC, Moore JN. 1990. Origin, structure, and evolution of a reattachment bar, Colorado River, Grand Canyon, Arizona. *Journal of Sedimentary Research* **60**: 982– 991 [online] Available from: http://archives.datapages.com/data/sepm/journals/v59-62/data/060/060006/0982.htm .
Web of Science® | Google Scholar | FullText@NAU

Rubin DM, Tate GB, Topping DJ, Anima RA. 2001. Use of rotating side-scan sonar to measure bedload. Proceedings of the Seventh Federal Interagency Sedimentation Conference, March 25 to 29, 2001, Reno, Nevada, 139– 144.
Google Scholar | FullText@NAU

Rubin DM, Topping DJ, Schmidt JC, Hazel JE Jr, Kaplinski M, Melis TS. 2002. Recent sediment studies refute Glen Canyon Dam hypothesis. *EOS, Transactions, American Geophysical Union* **83**: 273. https://doi-org.libproxy.nau.edu/10.1029/2002EO000191 .
Wiley Online Library | ADS | Google Scholar | FullText@NAU

Sabol TA, Topping DJ. 2013. Evaluation of intake efficiencies and associated sediment-concentration errors in US D-77 bag-type and US D-96-type depth-integrating suspended-sediment samplers. US Geological Survey Scientific Investigations Report 2012–5208: **88**. https://doi-org.libproxy.nau.edu/10.3133/sir20125208 Google Scholar | FullText@NAU

Sankey JB, Ralston BE, Grams PE, Schmidt JC, Cagney LE. 2015. Riparian vegetation, Colorado River, and climate: five decades of spatiotemporal dynamics in the Grand Canyon with river regulation. *Journal of Geophysical Research: Biogeosciences* **120**: 1532– 1547. https://doi-org.libproxy.nau.edu/10.1002/2015JG002991.Received .
Wiley Online Library | ADS | Web of Science® | Google Scholar | FullText@NAU

Sassi MG, Hoitink AJF, Vermeulen B. 2012. Impact of sound attenuation by suspended sediment on ADCP backscatter calibrations. *Water Resources Research*: 48.
https://doi-org.libproxy.nau.edu/10.1029/2012WR012008 .
Web of Science® | Google Scholar | FullText@NAU

Sauer VB, Meyer RW. 1992. Determination of error in individual discharge measurements. US Geological Survey Open-File Report 92–144 [online] Available from: http://pubs.usgs.gov/of/1992/ofr92-144/
Google Scholar | FullText@NAU

Schaffrath KR, Belmont P, Wheaton JM. 2015. Landscape-scale geomorphic change detection: quantifying spatially variable uncertainty and circumventing legacy data issues. *Geomorphology* **250**: 334– 348. https://doi-org.libproxy.nau.edu/10.1016/j.geomorph.2015.09.020 .
Crossref | ADS | Web of Science® | Google Scholar | FullText@NAU

Schimel ACG, Ierodiaconou D, Hulands L, Kennedy DM. 2015. Accounting for uncertainty in volumes of seabed change measured with repeat multibeam sonar surveys. *Continental Shelf Research* **111**: 52– 68. https://doi-org.libproxy.nau.edu/10.1016/j.csr.2015.10.019 .
Crossref | ADS | Web of Science® | Google Scholar | FullText@NAU

Schmidt JC. 1990. Recirculating flow and sedimentation in the Colorado river in Grand Canyon, Arizona. *The Journal of Geology* **98**: 709–724. https://doi-org.libproxy.nau.edu/10.1086/629435 .
Crossref | ADS | Web of Science® | Google Scholar | FullText@NAU

Schmidt JC. 1999. Summary and synthesis of geomorphic studies conducted during the 1996 controlled flood in Grand Canyon. In *The Controlled Flood in Grand Canyon*, RH Webb, JC Schmidt, RA Valdez, GR Marzolf (eds). AGU: Washington, DC; 329– 341. https://doi-org.libproxy.nau.edu/10.1029/GM110p0329
Wiley Online Library | Google Scholar | FullText@NAU

Schmidt JC, Graf JB. 1990. Aggradation and degradation of alluvial sand deposits, 1965 to 1986, Colorado River, Grand Canyon National Park, Arizona. US Geological Survey Professional Paper 1493: 74. [online] Available from: https://pubs.er.usgs.gov/publication/pp1493
Google Scholar | FullText@NAU

Schmidt JC, Grams PE. 2011. The high flows--physical science results. In *Effects of Three High-Flow Experiments on the Colorado River Ecosystem Downstream from Glen Canyon Dam, Arizona*, US Geological Survey Circular 1366, TS Melis (ed). 53–91. [online] Available from: https://pubs.usgs.gov/circ/1366/
Google Scholar | FullText@NAU

Schmidt JC, Grams PE, Leschin MF. 1999. Variation in the magnitude and style of deposition and erosion in three long (8–12 km) reaches as determined by photographic analysis. In *The Controlled Flood in Grand Canyon*, RH Webb, JC Schmidt, RA Valdez, GR Marzolf (eds). American Geophysical Union; 185– 203.
https://doi-org.libproxy.nau.edu/10.1029/GM110p0185
Wiley Online Library | Google Scholar | FullText@NAU

Schmidt JC, Rubin DM. 1995. Regulated streamflow, fine-grained deposits, and effective discharge in canyons with abundant debris fans. In *Natural and Anthropogenic Influences in Fluvial Geomorphology*, JE Costa, AJ Miller, KW Potter, PR Wilcock (eds). American Geophysical Union; 177– 195.
https://doi-org.libproxy.nau.edu/10.1029/GM089p0177
Wiley Online Library | Google Scholar | FullText@NAU

Schmidt JC, Wilcock PR. 2008. Metrics for assessing the downstream effects of dams. *Water Resources Research* **44**. https://doi-org.libproxy.nau.edu/10.1029/2006WR005092 .
Wiley Online Library | ADS | Web of Science® | Google Scholar | FullText@NAU

Shimizu Y, Giri S, Yamaguchi S, Nelson J. 2009. Numerical simulation of dune-flat bed transition and stage-discharge relationship with hysteresis effect. *Water Resources Research*: 45. https://doi-org.libproxy.nau.edu/10.1029/2008WR006830 .
Web of Science® | Google Scholar | FullText@NAU

Sibley D, Topping DJ, Hines M, Garner B. 2015. User-interactive sediment budgets in a browser: a web application for river science and management. In Proceedings of the 3rd Joint Federal Interagency Conference on Sedimentation and Hydrologic Modeling, April 19–23, Reno, Nevada, USA; 595–605. [online] Available from: http://acwi.gov/sos/pubs/3rdJFIC/Proceedings.pdf
Google Scholar | FullText@NAU

Slaymaker O. 2003. The sediment budget as conceptual framework and management tool. In *The Interactions between Sediments and Water*. Springer Netherlands: Dordrecht; 71– 82. https://doi-org.libproxy.nau.edu/10.1007/978-94-017-3366-3_12
Crossref | Google Scholar | FullText@NAU

Smith SW. 2003. *Digital Signal Processing: a Practical Guide for Engineers and Scientists*. Elsevier. **665**.
https://doi-org.libproxy.nau.edu/10.1016/B978-1-904275-26-8.50019-1
Google Scholar | FullText@NAU

Tarolli P. 2014. High-resolution topography for understanding earth surface processes: opportunities and challenges. *Geomorphology* **216**: 295– 312.
https://doi-org.libproxy.nau.edu/10.1016/j.geomorph.2014.03.008 .
Crossref | ADS | Web of Science® | Google Scholar | FullText@NAU

Taylor JR. 1997. *An Introduction to Error Analysis*, 2nd edn. University Science Books Sausalito, California.
Google Scholar | FullText@NAU

Thomas RB. 1985. Estimating total suspended sediment yield with probability sampling. *Water Resouces Research* **21**: 1381. https://doi-org.libproxy.nau.edu/10.1029/WR021i009p01381 .
Wiley Online Library | CAS | ADS | Web of Science® | Google Scholar | FullText@NAU

Thomas RB, Lewis J. 1995. An evaluation of flow-stratifed sampling for estimating suspended sediment loads. *Journal of Hydrology* **170**: 27– 45. https://doi-org.libproxy.nau.edu/10.1016/0022-1694(95)02699-P .
Crossref | ADS | Web of Science® | Google Scholar | FullText@NAU

Thorne PD, Meral R. 2008. Formulations for the scattering properties of suspended sandy sediments for use in the application of acoustics to sediment transport processes. *Continental Shelf Research* **28**: 309– 317. https://doi-org.libproxy.nau.edu/10.1016/j.csr.2007.08.002 .
Crossref | ADS | Web of Science® | Google Scholar | FullText@NAU

Topping DJ, Rubin DM, Grams PE, Griffths RE, Sabol TA, Voichick N, Tusso RB, Vanaman KM. 2010. Sediment transport during three controlled-flood experiments on the Colorado River downstream from Glen Canyon Dam, with implications for eddy-sandbar deposition in Grand Canyon National Park. US Geological Survey Open-File Report 2010–1128 [online] Available from: http://pubs.usgs.gov/of/2010/1128/
Google Scholar | FullText@NAU

Topping DJ, Rubin DM, Nelson JM, Kinzel PJ, Bennett JP. 1999. Linkage between grain-size evolution and sediment depletion during Colorado River floods. In *The Controlled Flood in Grand Canyon*, RH Webb, JC Schmidt, GR Marzolf, RA Valdez (eds). American Geophysical Union: Washington, DC; 71– 98. https://doi-org.libproxy.nau.edu/10.1029/GM110p0071
Wiley Online Library | Google Scholar | FullText@NAU

Topping DJ, Rubin DM, Nelson JM, Kinzel PJ, Corson IC. 2000a. Colorado River sediment transport 2. Systematic bed-elevation and grain-size effects of sand supply limitation. *Water Resources Research* **36**: 543– 570. https://doi-org.libproxy.nau.edu/10.1029/1999WR900286 .
Wiley Online Library | ADS | Web of Science® | Google Scholar | FullText@NAU

Topping DJ, Rubin DM, Vierra LE. 2000b. Colorado River sediment transport 1. Natural sediment supply limitation and the influence of Glen Canyon Dam. *Water Resources Research* **36**: 515– 542. https://doi-org.libproxy.nau.edu/10.1029/1999WR900285 .
Wiley Online Library | CAS | ADS | Web of Science® | Google Scholar | FullText@NAU

Topping DJ, Schmidt JC, Vierra LEJ. 2003. Computation and analysis of the instantaneous-discharge record for the Colorado River at Lees Ferry, Arizona -- May 8 1921, through September 30 2000. US Geological Survey Professional Paper 1677. Available from: http://pubs.usgs.gov/pp/pp1677/pdf/pp1677.pdf
Google Scholar | FullText@NAU

Topping DJ, Wright SA. 2016. Long-term continuous acoustical suspended-sediment measurements in rivers – theory, application, bias, and error. *US Geological Survey Professional Paper* **1823**. https://doi-org.libproxy.nau.edu/10.3133/pp1823 .
Crossref | Google Scholar | FullText@NAU

US Department of the Interior. 2007. Colorado River Interim Guidelines for Lower Basin Shortages and Coordinated Operations for Lake Powell and Lake Mead [online] Available from: https://www.usbr.gov/lc/region/programs/strategies/FEIS/
Google Scholar | FullText@NAU

US Department of the Interior. 2012. Environmental assessment: development and implementation of a protocol for high-flow experimental releases from Glen Canyon Dam, Arizona, 2011 through 2020. US Department of the Interior Bureau of Reclamation: Salt Lake City, Utah [online] Available from: https://www.usbr.gov/uc/envdocs/ea/gc/HFEProtocol/
Google Scholar | FullText@NAU

US Geological Survey. 1970. Quality of surface waters of the United States, 1965. Parts 9–11, Colorado River basin to Pacifc slope basins in California. Water Supply Paper 1965: 678. [online] Available from: https://pubs.er.usgs.gov/publication/wsp1965
Google Scholar | FullText@NAU

Vericat D, Batalla RJ. 2006. Sediment transport in a large impounded river: the lower Ebro, NE Iberian Peninsula. *Geomorphology* **79**: 72– 92. https://doi-org.libproxy.nau.edu/10.1016/j.geomorph.2005.09.017 .
Crossref | ADS | Web of Science® | Google Scholar | FullText@NAU

Walling DE, Webb BW. 1988. The reliability of rating curve estimates of suspended sediment yield: some further comments. Sediment Budgets (Proceedings of the Porto Alegre Symposium, December 1988) 337– 350.
Google Scholar | FullText@NAU

Warrick JA, Bountry JA, East AE, Magirl CS, Randle TJ, Gelfenbaum G, Ritchie AC, Pess GR, Leung V, Duda JJ. 2015. Large-scale dam removal on the Elwha River, Washington, USA: source-to-sink sediment budget and synthesis. *Geomorphology* **246**: 729– 750. https://doi-org.libproxy.nau.edu/10.1016/j.geomorph.2015.01.010 .
Crossref | ADS | Web of Science® | Google Scholar | FullText@NAU

Webb RH, Pringle PT, Rink GR. 1989. Debris flows from tributaries of the Colorado River, Grand Canyon National Park, Arizona. US Geological Survey Professional Paper 1492: 39. [online] Available from: https://pubs.er.usgs.gov/publication/pp1492
Google Scholar | FullText@NAU

Webb RH, Schmidt JC, Valdez RA, Marzolf GR. 1999. The Controlled Flood in Grand Canyon. RH Webb, JC Schmidt, GR Marzolf, RA Valdez (eds). *American Geophysical Union*: Washington, DC. https://doi-org.libproxy.nau.edu/10.1029/GM110
Wiley Online Library | Google Scholar | FullText@NAU

Wheaton JM, Brasington J, Darby SE, Sear DA. 2010. Accounting for uncertainty in DEMs from repeat topographic surveys: improved sediment budgets. *Earth Surface Processes and Landforms* **35**: 136– 156. https://doi-org.libproxy.nau.edu/10.1002/esp.1886 .
Wiley Online Library | Web of Science® | Google Scholar | FullText@NAU

Williams GP, Wolman MG. 1984. Downstream effects of dams on alluvial Rivers. US Geological Survey Professional Paper 1286: 83. [online] Available from: https://pubs.er.usgs.gov/publication/pp1286
Google Scholar | FullText@NAU

Williams RD, Brasington J, Vericat D, Hicks DM. 2014. Hyperscale terrain modelling of braided rivers: fusing mobile terrestrial laser scanning and optical bathymetric mapping. *Earth Surface Processes and Landforms* **39**: 167– 183. https://doi-org.libproxy.nau.edu/10.1002/esp.3437 .
Wiley Online Library | ADS | Web of Science® | Google Scholar | FullText@NAU

Wright SA, Kennedy TA. 2011. Science-based strategies for future high-flow experiments at Glen Canyon Dam. In *Effects of three high-flow experiments on the Colorado River ecosystem downstream from Glen Canyon Dam, Arizona*, TS Melis (ed), US Geological Survey Circular 1366; 127– 147 [online] Available from: http://pubs.usgs.gov/circ/1366/.
Google Scholar | FullText@NAU

Yang SL, Zhang J, Dai SB, Li M, Xu XJ. 2007. Effect of deposition and erosion within the main river channel and large lakes on sediment delivery to the estuary of the Yangtze River. *Journal of Geophysical Research: Earth Surface* **112**: 1– 13. https://doi-org.libproxy.nau.edu/10.1029/2006JF000484 .
Google Scholar | FullText@NAU

Citing Literature

Download PDF